

5-2018

Enhancing the Capabilities of Infrared Microscopy Apparatus

Ryan Wilmington

Follow this and additional works at: <https://scholarworks.wm.edu/honorsthesis>



Part of the [Condensed Matter Physics Commons](#), [Geometry and Topology Commons](#), [Numerical Analysis and Scientific Computing Commons](#), and the [Optics Commons](#)

Recommended Citation

Wilmington, Ryan, "Enhancing the Capabilities of Infrared Microscopy Apparatus" (2018). *Undergraduate Honors Theses*. Paper 1237.

<https://scholarworks.wm.edu/honorsthesis/1237>

This Honors Thesis is brought to you for free and open access by the Theses, Dissertations, & Master Projects at W&M ScholarWorks. It has been accepted for inclusion in Undergraduate Honors Theses by an authorized administrator of W&M ScholarWorks. For more information, please contact scholarworks@wm.edu.

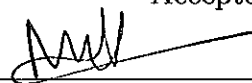
Enhancing the Capabilities of Infrared Microscopy Apparatus

A thesis submitted in partial fulfillment of the requirement
for the degree of Bachelor of Science with Honors in
Physics from the College of William and Mary in Virginia,

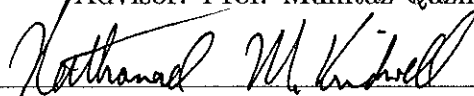
by

Ryan L. Wilmington

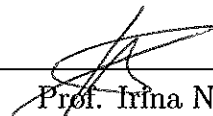
Accepted for Honors



Advisor: Prof. Mumtaz Qazilbash



Prof. Nathan Kidwell



Prof. Irina Novikova

Williamsburg, Virginia
May 2018

Contents

Acknowledgments	iii
Abstract	v
1 Introduction	1
1.1 Overview	1
2 Theory	4
2.1 Photon Spectroscopy	4
2.1.1 Apparatus	5
2.1.2 Spectrum Quality	7
2.2 Spot Size	8
3 Apparatus Design	14
3.1 The Optical Path	14
3.1.1 Spectrometer	15
3.1.2 Transfer Optics	15
3.1.3 Microscope	19
3.1.4 Detector	23
3.2 Optimization	25
3.3 Spot Size Measurement	29

3.4	Electronics	33
3.5	Pressure Systems	33
3.6	Dry Compressed Air Purge	34
3.7	Sample Translation Stage	37
3.8	Bolometer	38
4	Results and Conclusions	42
A	MATLAB Code Listings	44
A.1	Winston Cone	44
A.2	Knife Edge Technique	45
B	Winston Cone	51
B.1	Acceptance Angle	51
B.2	Alternative Calculation	54
B.3	Parabolic Mirror Selection	56

Acknowledgments

I would like to thank the Roy R Charles Center, National Science Foundation, and College of William & Mary department of Physics for honors fellow and summer research funding. I would also like to thank Dr. Mumtaz Qazilbash for advising my research project since summer 2016, as well as graduate students Tyler Huffman and Patrick McArdle who assisted in many experimental procedures and design considerations.

Abstract

My honors research consists of the design and optimization of a microscopy apparatus as an accessory to an existing macroscopic spectroscopy setup. Using this apparatus, spot sizes below 30 microns can be obtained with high enough intensity to measure infrared-active phonon features. In addition the main optical apparatus, I have developed electronic connections to interface to a mid-infrared detector, a purge gas housing to eliminate contamination from atmospheric vibrational resonances, and a sample stage with sub-micron precision translation to properly operate the apparatus in purge.

Chapter 1

Introduction

1.1 Overview

My research project centers on the expansion of experimental research capabilities for a microscopy and spectroscopy apparatus at the Photon Spectroscopy Laboratory at the College of William & Mary. The existing lab equipment has allowed for extensive research into many compounds ranging from Vanadium dioxide to brown recluse spider silk. However, the use of a macroscopic spectrometer alone creates a sample resolution limitation. If a sample is much smaller than the spectrometer's spot size, it may not absorb enough light to be noticeable on a transmission spectra. Additionally, a larger sample must be very uniform at macroscopic scales to be appropriately measured. If the sample is inhomogeneous, it is difficult to determine if an optical feature belongs to the whole sample, or just to subregions in the material. Imagine for instance, trying to determine the color of a zebra if the human eye could only resolve a one-foot spot. From our blurry perspective, we might say that the zebra is grey, because we have "averaged" the two different stripes of a zebra into one image. However, with a one-centimeter spot size, we might easily say that a zebra has some regions of black coloring, and some of white, but none that are grey! We have misunderstood the zebra simply because we lacked the necessary

resolution. Infrared spectroscopy is very much the same battle. To distinguish the unique features of inhomogeneous or anisotropic material, we must be able to resolve regions on the same order as the inhomogeneities in our sample!

In summary, the implementation of an infrared microscope allows not only for more precise data on existing samples to be taken, but also for a whole new class of micron-scale samples to be analyzed.

To achieve this microscopy integration, I have three distinct research goals. I intend to:

1. Optically and electronically connect a Fourier Transform Infrared (FTIR) Spectrometer to an Infrared Microscope
2. Optimize microscope throughput intensity and spot size for high signal-to-noise sub-50 micron sampling
3. Add three additional key improvements to the microscopy apparatus: an additional optical path to a Bolometer detector to expand spectral sampling range, a purge gas housing to remove signal contamination, and an adjustable sample stage to allow for sub-micron precision sample translation.

The first phase was primarily focused on surmounting the challenges involved in manually pairing two optical and electronic devices not designed for use with each other. This process involved the design of new transfer optics, kinetic vacuum-system adapters, and custom connecting electronics.

Next, the microscope was optimized from a base level of functionality toward the highest possible levels of performance. After establishing viability of the apparatus, it was necessary to improve the optical quality of the microscope beampath so that the best possible data can be obtained. Primarily, this optimization focused on minimizing the sample spot size while also maximizing the intensity throughput.

To detect phonons in the same spectral range as atmospheric vibrational and rotational resonances from CO_2 and H_2O , a purge gas enclosure was constructed and optimized. To ensure data is reliable in these regions, it was necessary to show with 100% lines (see section 2.1.2) that any remaining phonon contamination was less than the noise level of the detector.

To fully expand the capabilities of the apparatus, it will be necessary to use multiple detection techniques. As was done with the original spectroscopy apparatus, a Bolometer detector will be used to increase the measurable spectral bandwidth. With this addition, the entire infrared spectrum will be accessible for analysis.

Finally, after finalizing the microscope optimizations and improvements, I performed the first measurement of a test sample. This experiment served to test the practical viability of my new apparatus, and showed that the microscopy apparatus could roughly recreate sample data taken with the existing spectroscopy apparatus.

Rather than for personal, non-repeatable use, my research project is designed for continued use in the Photon Spectroscopy Lab at William & Mary. Once fully operational, this microscopy apparatus can be used by many future generations of graduate and undergraduate students in conjunction with the existing spectroscopy equipment to expand the possibilities of spectroscopy research at William & Mary.

Chapter 2

Theory

While the core of my time spent over the last year has focused on the design of my experimental apparatus, there are several critical topics I have explored to prepare for various stages of the design process. First, I will discuss photon spectroscopy as it relates to my apparatus. Next, I will give an overview of the theoretical limits of the microscope's spot size, which guides the optical optimization process.

For a discussion on the Winston Cone, a type of Compound Parabolic Concentrator (CPC) that is used as a light collector for the 4.2/1.6K Bolometer detector element, please see the corresponding chapter in the Appendix.

2.1 Photon Spectroscopy

Photon spectroscopy is an experimental technique used in a variety of fields to identify properties of material based on a detected response to incident photons. An important application of infrared spectroscopy is the study of infrared-active phonons in the atomic lattice of a material. Observed phonons of a given frequency correspond to atomic vibrational resonances of the sampled material, which are a direct result of that material's lattice structure. A material will only absorb photons at its precise phonon frequencies, so all other wavelengths are reflected and/or transmitted. If the frequencies present in the final light spot with and without the sample can be detected

and compared, then the phonons of a material can be directly measured.

2.1.1 Apparatus

First, a light source must be selected which spans the appropriate spectral range. In general, light source spectral ranges can be roughly sorted between near-infrared (NIR), mid-infrared (MIR), and far-infrared (FIR) wavelength ranges. These ranges are tabulated below in table 2.1 by wavelength and by wavenumber (the preferred unit for infrared spectroscopy).

Table 2.1: Infrared Wavelength Ranges

	NIR	MIR	FIR
Wavelength (μm)	0.8 - 2.5	2.5 - 25	25 - 1000
Wavenumber (cm^{-1})	14000 - 4000	4000 - 400	400 - 10

Modern Fourier Transform Infrared (FTIR) spectrometers use an interferometer and Fourier analysis software to analyze many different frequencies simultaneously. An interferometer (with a beamsplitter transmissive in the selected IR range) uses a moving mirror to form a spectrum of wavelengths. The resulting beam can be detected as an interferogram plot of intensity vs time (with periodicity corresponding to the rate of the moving mirror). A Fourier transform of this interferogram can parse each individual sinusoidal component, each of which encodes the intensity of the transmitted light of a given frequency. A plot of these frequencies vs intensity gives the full spectrum of the detected light. An example of an interferogram and frequency spectrum is given in figure 2.1.

As the incident light passes through the sample, resonant frequencies are excited. These absorption features appear as valleys (lower intensity) in a reflectance or transmission spectrum. To extract the absorption spectrum of the sample itself, it is necessary to compare a background spectrum (no sample) and a sample spectrum.

Dividing the sample spectrum with the background spectrum shows the transmission spectrum of the sample. By subtracting this spectrum from one, an effective "absorbance" plot is formed that shows all frequencies that decreased in intensity as spectral peaks. These peaks directly indicate any phonon resonance frequencies. Although in practice one minus the transmission is often referred to as an absorbance plot, to obtain the real absorption spectrum it is important to also consider the reflectance of the sample, to find which frequencies are neither reflected nor transmitted.

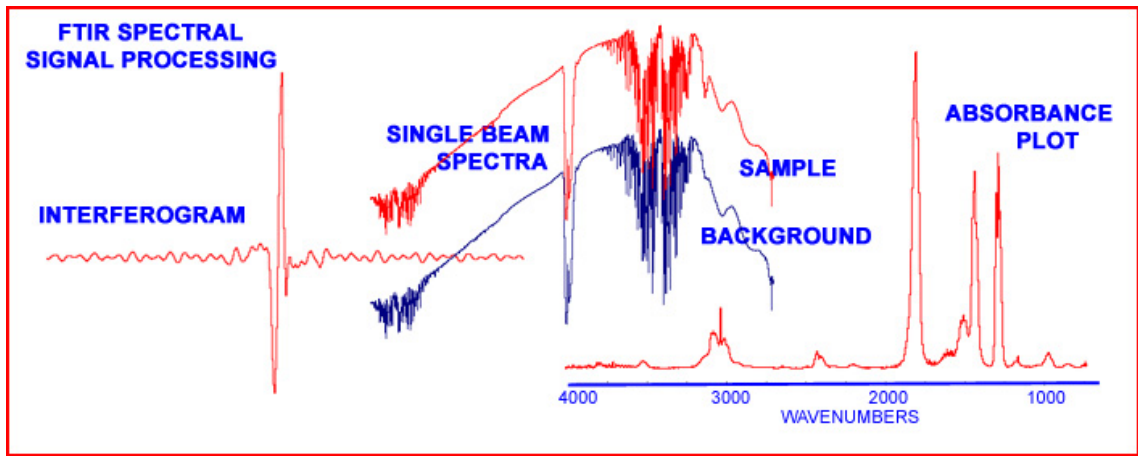


Figure 2.1: Graphic of IR Signal as Interferogram, Spectrum, and Spectra Plot

To obtain the interferogram of the transmitted or reflected light after the sample, reflective optics can be used to direct the beam into a photodetector. As the detector element size is often very small (fractions of a millimeter), the beam must come to a tight focus at the detection plane to maximize the intensity of the produced spectrum. Increasing the amount of light directed onto the detector element and improving the quality of the optical beam both increase the signal to noise ratio, allowing for more certainty in detected phonons.

2.1.2 Spectrum Quality

In spectroscopy, the sample is never the only thing that will appear in a transmission spectrum. While some absorption occurs at the sample, incident photons can also be absorbed by anything in the beampath before the detector. For example, a "transparent" optical window will actually have a spectrum of transmission intensity. Similarly, mirrors may only be reflective for a certain range of frequencies, and the reflectance may not be uniform across that range. Sources for visible and infrared light have a natural spectrum which tapers off toward zero at the edges of the produced frequency range.

Additionally, the medium through which the light travels will also cause some absorption to occur. Ideally, the entire optical beampath is in vacuum so only the sample provides phonons that are detected. However, a more realistic model of the spectrometer's behavior includes the presence of certain contaminants. The two most significant atmospheric contaminants for the infrared are water vapor and carbon dioxide, both of which have infrared-active vibrational modes. To remove these signals, the optical beampath must be purified as much as possible. A vacuum chamber or purge gas housing are possible solutions that diminish the presence of H_2O and CO_2 in the spectrum data (both of which are used in my apparatus).

Additionally, electrical and mechanical noise sources can disrupt the data if their resonance frequencies overlap with the examined spectral range. Fans, wiring, pumps, and other typical lab equipment can produce undesirable frequencies, so it is critical to identify any noise sources before taking data. A "100% line" is a measure of a background spectrum divided by another background spectrum to measure any prominent fluctuations in the beampath environment. A perfectly ideal measurement would so a 100% line equal to one across the entire measured spectral range. In practice, as the measured region approaches the extremes of the detector's spectral

range, the noise level deviating above and below one will increase. Also, if significant variable contamination exists (like H₂O and CO₂ in the air), spectral peaks will appear at the location of the resonance frequencies of these contaminate molecules. Additionally, noise sources can be hugely variable and thus are often easily spotted as precise peaks in the 100% line. Once identified, the noise source can be removed if possible or dampened (with an electronic filter or with a physical material like a rubber pad). If the noise source is intrinsic to the apparatus itself (i.e. the preamp circuitboard), then it is sometimes possible to remove the precise noise frequency with a digital filter after data is collected. In some cases, noise sources appear equally in both sample and background measurements, however oftentimes noise sources such as atmospheric contamination are not consistent between scans, and therefore appear as a 'variation' between the background and sample scan. These types of noise sources are the most critical to eliminate. If the noise produces even variation about a central position over short timescales, it is possible to average over multiple measurements in succession to partially remove the noise. However, there is a balance that must be found between taking data long enough to remove noise sources, and not taking data so long as to introduce drift in the sample position, purge air conditions, or other factors.

2.2 Spot Size

The terminology for discussing spot sizes and apertures varies greatly between sources, so to avoid confusion I will define my terms as follows: "Aperture" refers to the removable confocal pinhole, placed at a conjugate plane to the objective focal plane. This microscope has two (one before sample, one after sample) 1.5mm removable apertures, a method called "redundant aperturing" (see discussion below). Other terms used to describe apertures include confocal pinholes, field stops, and remote

image masks. “Diffraction Limited Spot” (DLS) refers to the smallest possible spot size for ideally aligned optics given the numerical aperture (N.A.) of the objective and the wavelength of light used. Given a beam has a Gaussian distribution of light intensity, different Fraunhofer minimums will give different portions of the focus spot. For example, the distance between the first two dark minimums of the diffraction pattern is called the Airy Disk, and contains 84% of the light intensity [4]. The IR Plan Reflachromat objective has a 15X magnification and 0.58 N.A., so for our purposes the DLS size will be a diameter assuming a 0.58 N.A. for a specified wavelength and Fraunhofer minimum. “Sampling Area” refers to the region of the sample observable given any particular aperture used. The sampling area is determined by the reverse magnification of the aperture on the sample. Our upper aperture has a diameter of 1.5mm, which when divided by 15 gives the effective sampling area of 100 microns*. *Note that the sampling area and all measurements above are given as diameters. Unless specified otherwise, all measurements are to be interpreted as the diameter of a circular area.

The main purpose of the aperture in the confocal plane is to improve spatial definition of the sample plane. By placing an aperture at the point where the light before the sample should come to a minimum, stray out-of-focus light can be obstructed. However, the aperture itself, in addition to the source and the sample, also diffracts light. In theory, the use of two apertures, or “dual remote image masks” can be used to eliminate this diffuse light, while retaining a majority of the airy disk intensity. In reality, the first aperture is much more vital than the second, which is largely used for condenser alignment, but in the case where diffraction is the limit of spatial resolution, then redundant aperturing can improve spatial definition.

As is evident from the figure 2.2, the use of two apertures has two effects on the signal. The slope of the edge signal line is increased, which indicates minimized

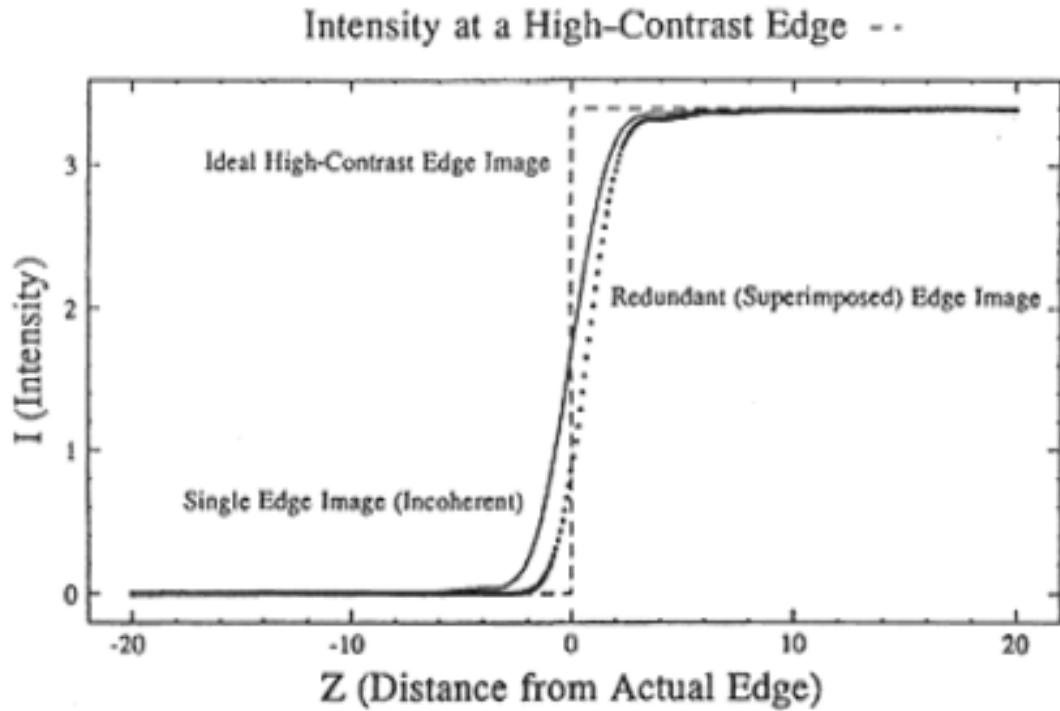


Figure 2.2: Two Unobstructed High-Contrast Edge Graph

diffraction and improved spatial definition. Also, the overall intensity has decreased. This tradeoff, and why the two aperture method ultimately gained traction, are discussed in Practical Guide to Infrared Microspectrometry [2]. According to the text, at one point most literature on microscopy recommended not using two apertures to avoid loss of intensity. However, the later consensus was that double aperturing did not result in heterogeneous energy loss, but rather that it cut most intensity from the most diffuse regions of the spot. As a result, double apertures can be effectively implemented to improve spatial resolution.

While discussion over the use of dual apertures is largely settled, there is an alternative method to apertures used to improve spatial resolution, which is the use of objectives with increased numerical apertures.

A higher N.A. effectively flattens the light angle on the sample, which decreases

the impact of stray light. However, the change of N.A. also effects the depth of field and working distance for the microscope. A larger incident angle increases the amount by which the focus shifts for each unit of vertical translation, so less sample depth is in focus for any given measurement. Naturally, this also means the sample must be closer to the objective to be in the focal plane, which potentially limits the thickness of the sample and substrate.

Alternatively, using two apertures and a smaller N.A. objective results in less intensity throughput to the detector, and aligning both apertures correctly is essential (and difficult for variable apertures). That aside, the spatial resolution can be improved without decreasing the depth of field or working distance. For reference, the text considers the good range of low to high N.A. values being from 0.5 to 0.71, and our IR Plan Reflachromat Objective has a 0.58 N.A. (and two apertures).

The diffraction limited spot, DLS, is given by equation 2.1,

$$d = \frac{m\lambda}{N.A.} \tag{2.1}$$

where d is the DLS diameter, λ is the wavelength, N.A. is the numerical aperture, and m is a variable dependent on the shape of the aperture and the minimum in question. Slit apertures have integer m values, but not for circular apertures. The theoretical diffraction-limited distance between first order minimums (called the Airy Disk) is given by $m = 1.220$ (first Fraunhofer minimum). The first four minimums, m values, and corresponding spot sizes in terms of wavelength for a 0.58 N.A. are given in the table below.

Table 2.2: Diffraction Limited Spot Sizes for 'nth' Fraunhofer Minimum

n	1	2	3	4
m	1.220	2.233	3.238	4.241
λ	2.103	3.850	5.583	7.312

where λ , n , and m are defined as per equation 2.1.

For any given wavelength, our microscope's DLS for 84% intensity is 2.1λ , and for 99% intensity is 7.3λ .

A more complete picture of the IR Plan DLS is given in figure B.1.

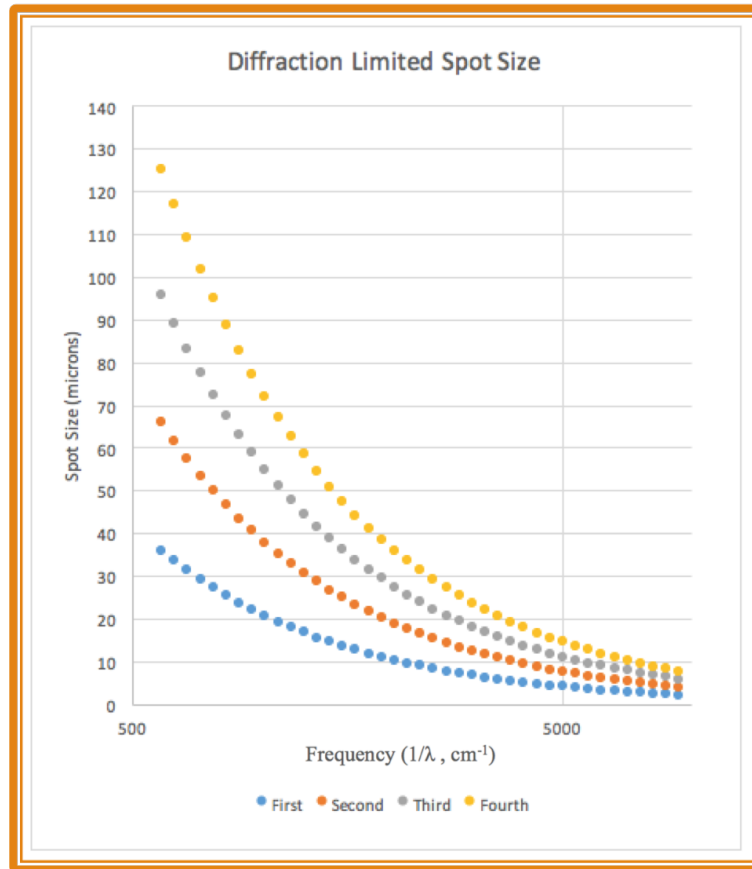


Figure 2.3: Diffraction Limit Spot Sizes for Fraunhofer Minima at Varying Wavelengths

The DLS, and the variation between 84% and 99% intensity is highly dependent upon the wavelength, especially in the MIR/FIR.

As mentioned before, the sampling area is defined by the aperture used and magnification of the objective. For a 1.5mm aperture and a 15X objective, the sampling area is 100 microns. To choose an appropriate aperture, one must consider the DLS, sample size, and intensity throughput. The sampling area should be larger than the

DLS, but not larger than the sample size. If the aperture is such that the sampling area is within the DLS, the diffraction effect of the aperture is increased and spatial resolution is diminished. For example, a 1.5mm aperture avoids the DLS in the NIR and MIR, but cuts off some intensity in the FIR. To get 99% throughput (capture the fourth Fraunhofer minimum) it may be necessary to use a larger aperture in the FIR region. At the other limit, the aperture only improves spatial definition if stray light at the confocal plane is blocked, to the point where too large an aperture is (intuitively) equivalent to no aperture at all.

Chapter 3

Apparatus Design

The bulk of my honors thesis represents the design, construction, and optimization of my custom microscopy apparatus. Although the design process is very iterative and non-linear, I have attempted to sort each specific design contribution to my project within a larger category. For each aspect of the apparatus, I will demonstrate its purpose, connection to the rest of the experimental setup, and practical implementation.

3.1 The Optical Path

For any optical apparatus, the primary concern must first be the optical path itself. The main question to be answered is: “How will I properly direct the appropriate wavelengths and intensity of light into my infrared microscope, such that a minimal spot size may be achieved?”

The quality of the light, proper alignment of any directing optics, removal of aberration, and maximization of intensity are all omnipresent concerns. Additionally, every small beam defect in the earliest part or “upstream” of the beampath will have a proportionate effect on all optics afterward or “downstream”.

A summary of the optical beampath, which will be expanded upon in the following sections, is as follow: The output from an FTIR spectrometer travels through a series of reflective optics to resize and redirect the beam toward the optical input of an

infrared microscope. Once properly aligned, the beam is brought to a focus at the sample plane, and then directed and refocused onto the element of a detector. If necessary, an additional set of transfer optics can be installed to direct the beam to an alternate detector with a different spectral bandwidth.

3.1.1 Spectrometer

My project relies on a Bruker Vertex 80v FTIR spectrometer. For a general measurement, we use a MIR source with a KBr beamsplitter in the interferometer portion of the spectrometer to form our source beam. For a larger discussion on the physics of the spectrometer, please see the Spectroscopy section in the Theory chapter.

3.1.2 Transfer Optics

The output of the interferometer portion of the spectrometer forms a roughly collimated two-inch diameter beam, which is directed toward a parabolic mirror. For standard spectrometer operation, this parabolic mirror would direct the light source into a sample chamber within the spectrometer itself. However, for the microscopy apparatus I wanted to direct the beam out of the spectrometer altogether. Additionally, the IR input beam diameter for the microscope must be about one inch, so the beam would need to be resized.

To accomplish this, I planned to use two parabolic mirrors of different focal lengths to capture the beam, and produce a collimated beam of a different diameter. Finally, I would use a plane mirror to direct the beam into the microscope input. All of these would be placed in an accessory chamber of the spectrometer itself, shown in figures 3.1 and 3.2. An outline of my design process was as follows:

1. Precisely measure the 3D dimensions of the spectrometer chamber
2. Design and produce machining schematics for two plates to hold optical mounts

3. Design and construct optical mount setup for three reflective mirrors and an iris
4. Align all transfer optics to preserve beam circularity and collimation, avoid clipping, and properly direct the beam into the IR input of the microscope

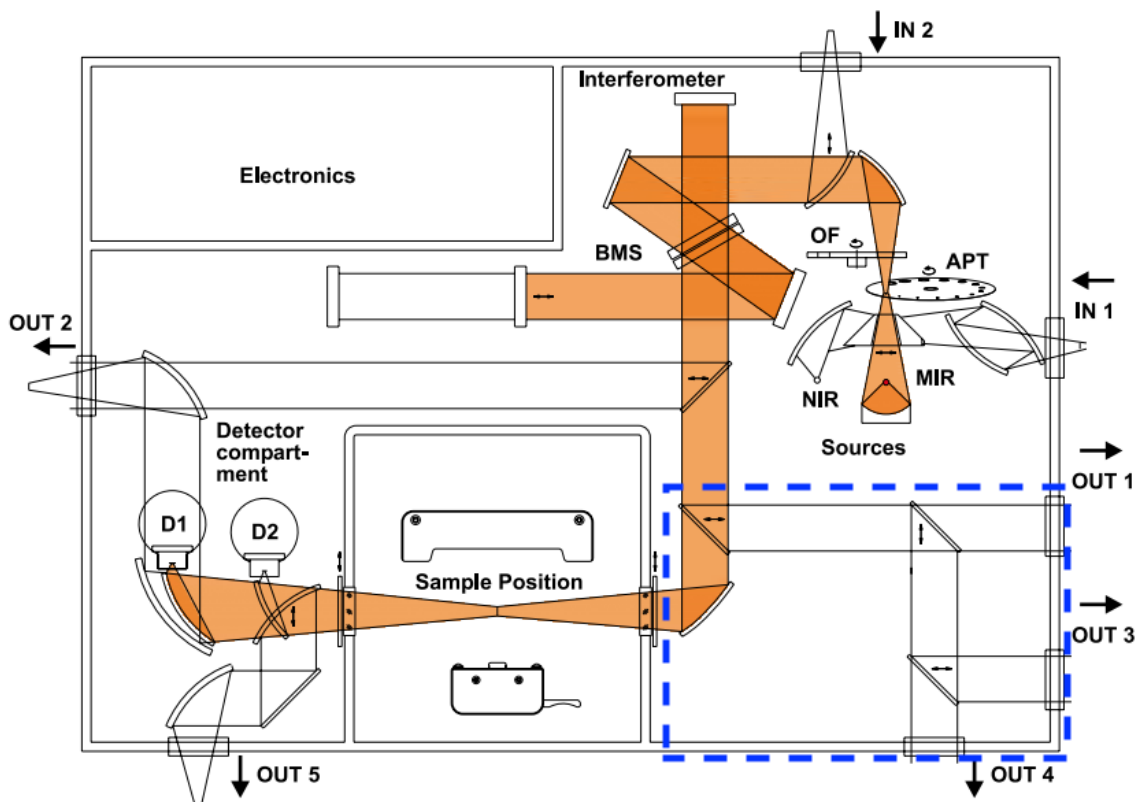


Figure 3.1: Layout of Bruker Vertex 80v Spectrometer

(blue dashed line indicates the sample accessory chamber, orange indicates the unmodified beam path)

First, completed my measurements of the sample chamber, which were then formed into a digital recreation of the sample chamber using Solidworks 3D CAD software. From the 3D model I mapped out the ideal beam path through the chamber. Then, I designed mounting plates that could hold the optical mounts in place, and connect to the existing threads in the spectrometer floor. I created models of

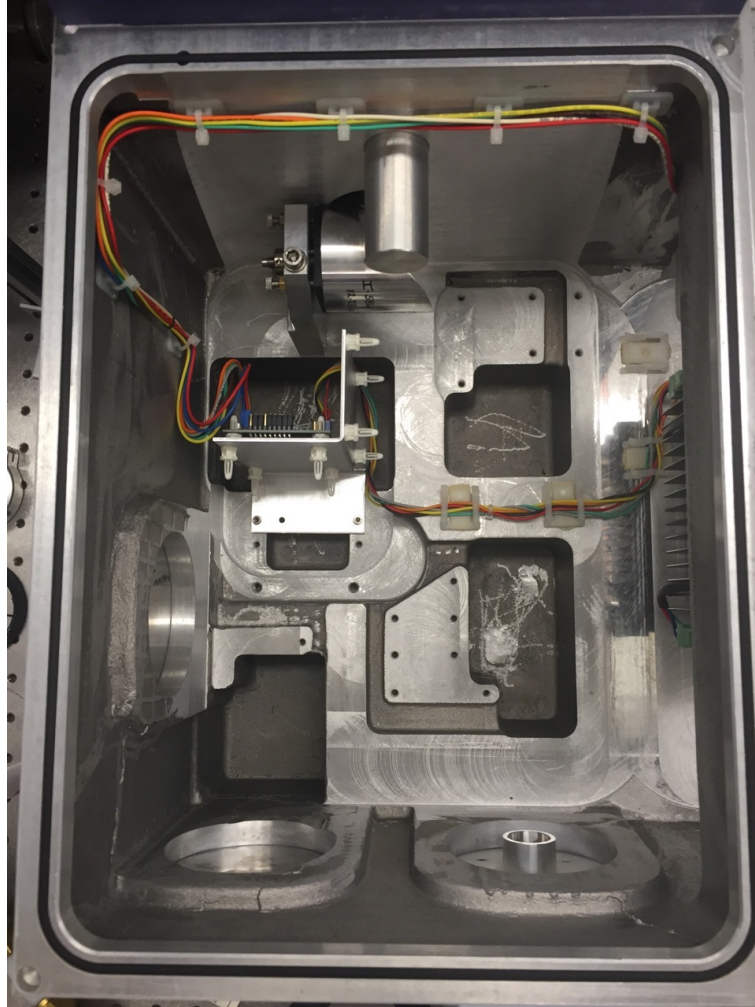


Figure 3.2: Image of Spectrometer Accessory Chamber (before modification)

my intended plate design based on the ideal position of each mirror, as well as the obstacles present in the spectrometer chamber. After an iterative review process, I finalized a machine drawing for each plate and had both constructed from aluminum.

The mirrors were selected based on several factors. To resize the beam, two off-axis parabolic (OAP) mirrors were used: one with a four-inch focal length and two-inch diameter to capture the beam, and the other with a two-inch focal length and a two-inch diameter. Between the two, a 5mm iris was to be placed. The two OAPs together brought the beam to a focus at the focal length of each mirror, and after the

second mirror a one-inch collimated beam was produced. The final plane mirror is used to direct the beam out of “port 3” on the spectrometer and into the microscope IR input. All mirrors use a bare aluminum coating, which is near 98% reflective in the visible, MIR, and FIR, making it ideal for many potential applications of the apparatus.

Next, I selected optical mounts appropriate to the degrees of freedom necessary to align each mirror, and found appropriate hardware to secure each mirror at the proper beam height relative to the chamber floor. The design plan for the mounting of each mirror is shown in figure 3.3.

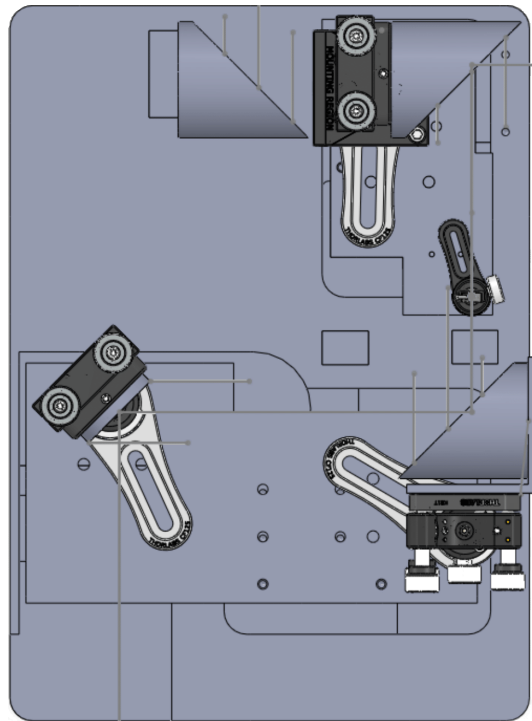


Figure 3.3: Spectrometer Accessory Chamber Transfer Optics Plan

(Top Left) parabolic mirror for the unmodified beampath (Top Right) four-inch focal length OAP (Center Right) 5mm iris (Bottom Left) plane mirror (Bottom Right) two-inch focal length OAP

After the plates were machined and mounts and mirrors ordered, the transfer optics assembly was installed. To align the mirrors we had to ensure each mirror

was at the appropriate optical height. Each mount used two or three fine adjusts for yaw, pitch or roll. The first mirror was aligned at 90 degrees to the incoming beam, directing the two-inch diameter beam to a small focus at the iris. The second parabolic mirror was aligned treating the iris spot as a point source, and collimating the beam again at half the size (one-inch diameter). This collimated beam, now the right size for the microscope input, is reflected at 90 degrees from the second OAP and again at 90 degrees by the plane mirror into port 3 of the spectrometer. At each phase, it was necessary to visually check the beam's divergence and shape to ensure minimal aberrations were introduced.

3.1.3 Microscope

The microscope used in my apparatus is a Spectra-Tech IR Plan Advantage. Unlike the Bruker Vertex spectrometer, the microscope is an older, all-manual design from a different manufacturer. There are no lenses, the entire beampath (including the objective) is formed with reflective optics. The only electronic interface is from the detector pre-amp board, which will be discussed in the next section. An image of the microscope is shown in figure 3.4.

The microscope has visual and infrared modes for both reflective and transmissive sampling. However, each of these beampaths have significant overlap, with a few manual sliders serving to move critical mirrors for different beampath options. While the entire beampath is quite complex, the key stages within the microscope are summarized below. For a full diagram of the beampath for reflectance and transmission, see figures 3.5 and 3.6.

For simplicity, I will describe the IR modes of the microscope only, however the visual modes are very similar with two main modifications. Instead of an infrared input source, a halogen lamp is used as a point visible source, directed to the sample

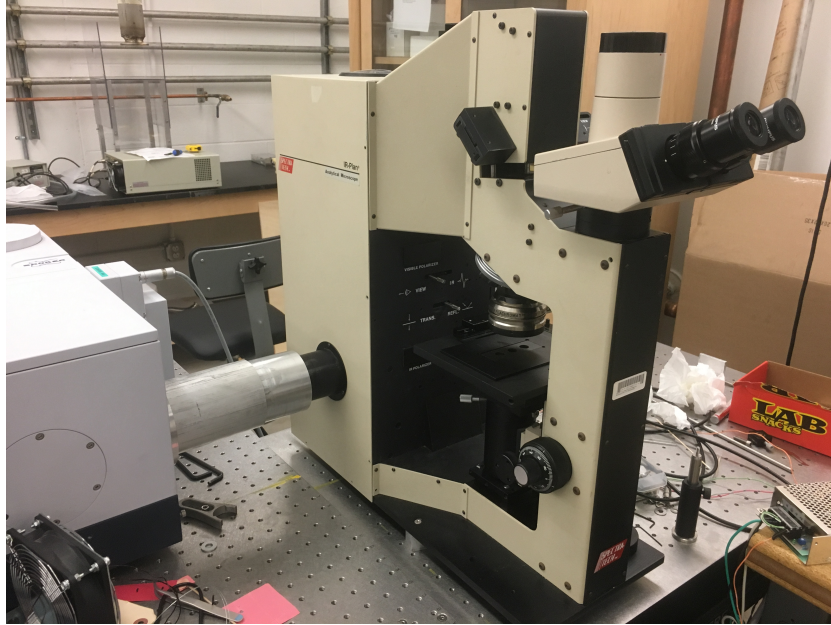


Figure 3.4: Spectra Tech IR Plan Advantage Microscope
(Shown in final position on optical table, coupled to Bruker spectrometer)

plane by a separate set of reflecting mirrors. After transmitting through or reflecting from the sample plane, the light beam is directed toward the upper eyepieces, where it can be viewed directly.

For an IR input, there is an input off-axis concave hyperbolic mirror that captures the incoming one-inch diameter collimated beam, and creates a converging beam which is directed to several plane mirrors. After reflecting twice and reaching a focus, the now diverging beam is reflecting up to an ellipsoid mirror, which focuses the beam onto the upper aperture confocal plane (above the objective). In transmission mode, the entire beam is captured by the ellipse. However, in reflectance mode half the beam is blocked, so that one side of the ellipse can be used for outgoing light to the sample, and the other half of the ellipse can act as the downstream collecting mirror for reflected light.

After the first ellipse, the light is roughly focused at the upper aperture confocal

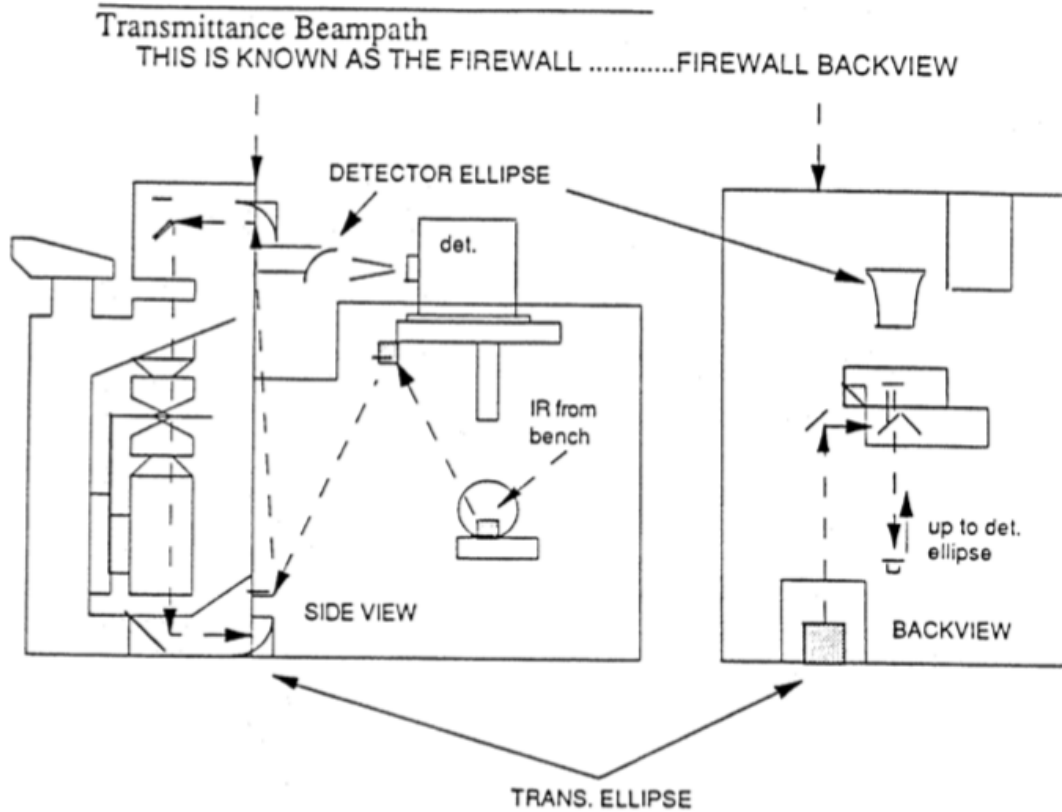


Figure 3.5: Microscope Transmission Beampath

plane. An aperture placed here will define the optical field, and also limit the sample spot size. A smaller spot size allows more precise measurement of sample regions, which is critical for small samples. However, the aperture will decrease throughput intensity of the IR beam by an amount roughly proportionate the the aperture size (the beam intensity distribution is roughly Gaussian, not uniform, so the relationship between aperture size and intensity is not strictly linear. A discussion of the details of these two factors and how they are balanced is given in the Optimization section, and the microscope's best functionality for various aperture settings is given in the Results chapter. For reference, a 1.5mm aperture magnified 15 times forms a $100\mu m$ optical field.

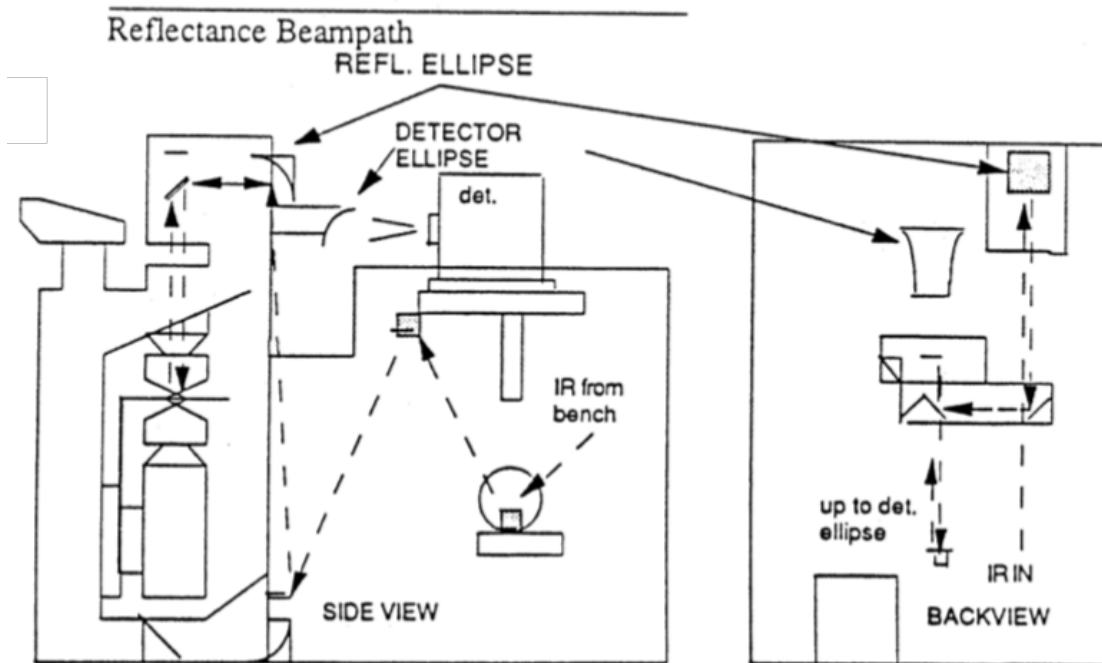


Figure 3.6: Microscope Reflectance Beampath

Following the first aperture is the objective, which is a 15X Schwarzschild-model Reflachromat. Schwarzschild objectives are an all-reflective magnifying element which uses two mirrors to direct a beam to a tight focus with a large solid angle (see figure 3.7). The diverging input from the light source (set by the aperture at the confocal plane) hits a convex secondary mirror, is then back-reflected onto a larger, concave primary mirror. This mirror has a short focal length, and therefore a large numerical aperture (N.A.), coming to a tight spot at the sample plane. This mirror contains a hole allowing the incident light to reach the first secondary mirror along the optical axis, resulting in some of the back-reflecting light exiting the objective toward the upper aperture, resulting in some lost intensity.

If the microscope is in reflectance mode, the beam now returns the way it came, coming back through the objective, upper aperture, and hitting the opposite side off

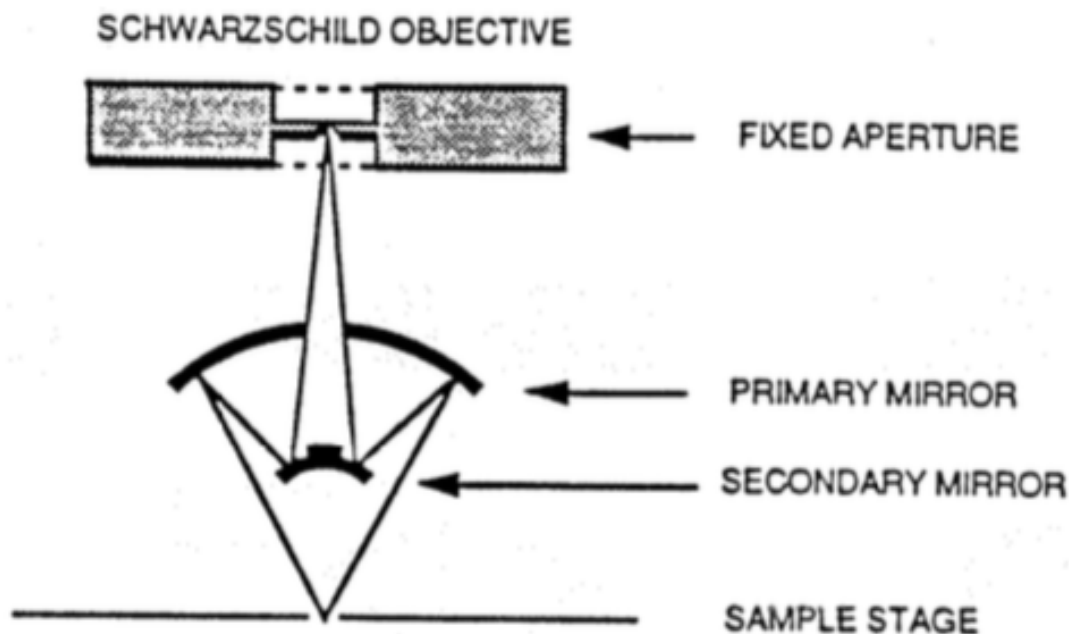


Figure 3.7: Schwarzschild Objective Diagram

the first ellipse. From there, it is reflected from several plane mirrors into the detector ellipse, which focuses the beam onto the detector element.

Transmission mode is similar, except instead of passing back up toward the upper aperture, the beam is directed into a condenser (of the same design as the 15X objective). The condenser backfocuses onto a lower aperture, forming a spot at the lower confocal image plane. From there, an ellipse captures the diverging beam, which is reflected off several plane mirrors into the final detector ellipse, and onto the detector element.

3.1.4 Detector

The infrared detector I am using is an Thermo-Nicolet MCT/A detector with a 0.25mm x 0.25mm element. The detector is liquid nitrogen cooled and is sensitive from around 8000 to 500 cm^{-1} . The detector was originally positioned directly on a

platform inside the microscope shell, however I required that the detector be easily removable and replaceable so it could be exchanged for an additional Bolometer detector. To that end, I designed an interchangeable baseplate which can be secured inside the microscope shell. By securing the detector to the baseplate, multiple detector options can be conveniently exchanged for a given experiment.

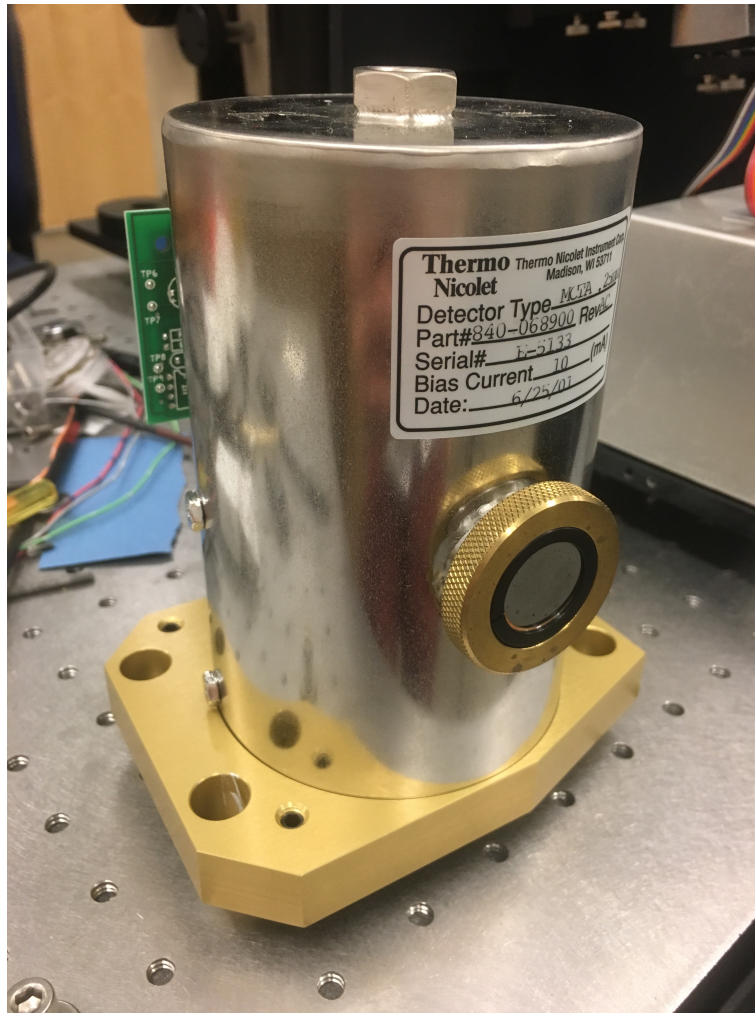


Figure 3.8: MCT Detector, Detector Window Side
(shown uninstalled from microscope)

The detector has a raw output signal that is amplified by a pre-amplifier circuit-board. This board will be discussed in the Electronics section.

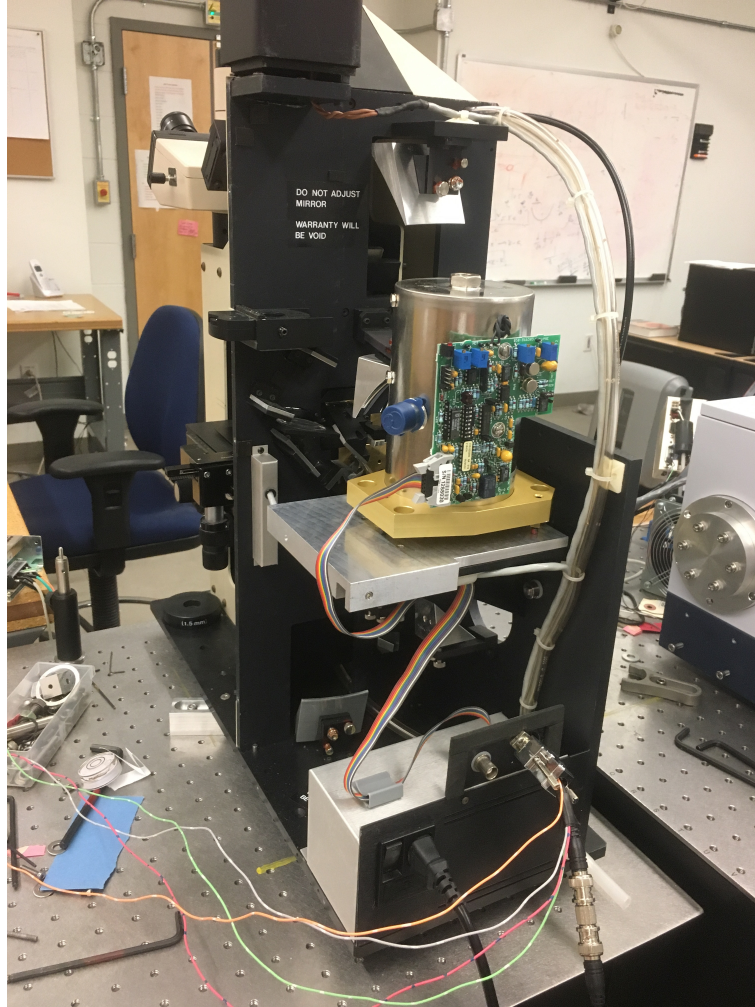


Figure 3.9: MCT Detector, Pre-Amplifier Side

(shown installed inside microscope, mounted on interchangeable baseplate)

3.2 Optimization

The entire goal of infrared microscopy is apply infrared spectroscopy to sub-macroscopic samples. Naturally, it is of extreme interest to minimize the necessary size of a given sample, and thus minimize the effective size limit of testable materials. To do this, the IR spot size at the sample plane must be decreased, while maintaining sufficient throughput intensity so that the signal-to-noise values are reasonable. One source of

intensity loss previously mentioned is the upper aperture prior to the objective. At this confocal plane, the spot size is largely determined by the aperture size, which also determines the final measurable intensity.

To increase intensity, the spot at the upper aperture should be as small as possible, so that the upper aperture clips a minimal amount of light to form the optical sample field. To ensure that a collimated IR input beam truly provides the best possible spot size at the sample plane, a series of measurements were taken using a 7/8-inch beam HeNe laser source. The laser source uses a lens collimator which can be adjusted, allowing a range of divergent and convergent beams to be tested.

For each lens collimator position, the divergence/convergence angle was measured by measuring the beam diameter at known lengths along the optical axis. Then, the laser was aligned to the IR input of the microscope, and the beam spot size at the upper aperture was roughly measured using a card. The resulting data is plotted in figure 3.10.

As the microscope's upper aperture slot is largely obscured, consistent measurement was difficult. However, the general trend of a large number of measurements shows the ideal IR input beam falling either right on or just below a perfectly collimated beam. This matches the expectation based on the conic constant of a concave hyperbolic mirror.

A brief note on conic sections and curved mirrors: The conic constant of a curved surface is a representation of its curvature. A perfect circle is represented as a zero, with oblate ellipses represented as greater than zero, and prolate ellipses as fractions between zero and -1. A parabola ranges between -1 and -2, with all lower values representing hyperbolas until negative infinity, which is a flat plane. A hyperbolic mirror accepts a convergent beam, and an ellipsoidal mirror accepts a divergent beam. The parabolic mirror represents the dividing line between these two reflective optics,

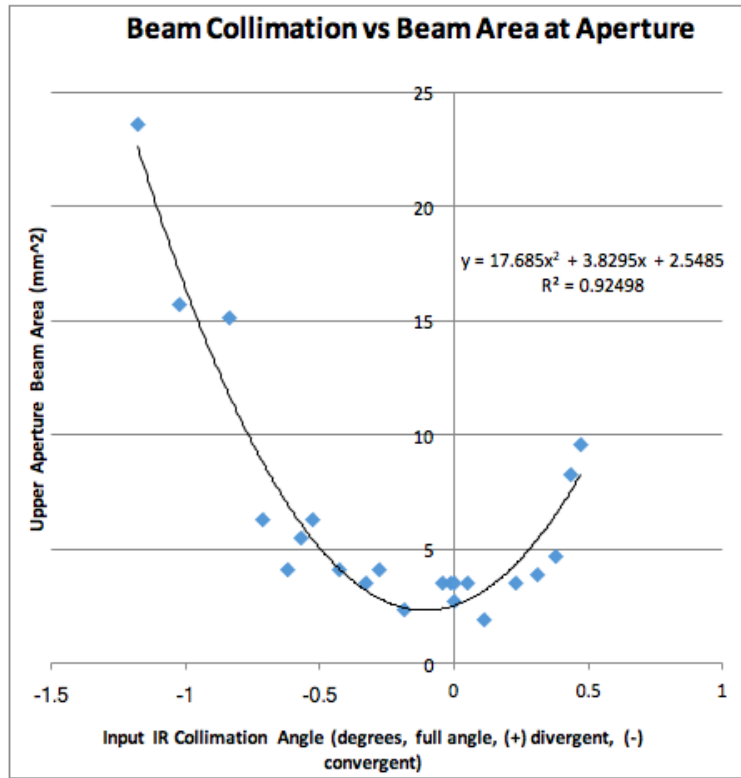


Figure 3.10: Beam Collimation vs Upper Aperture Spot Size Measurement

with a conic constant of -1. The conic constants of various conic sections are plotted in figure 3.11. The ideal parabolic mirror accepts a perfectly collimated beam. All three mirrors produce a convergent beam, which comes to a focus at the reflected focal length.

In addition to optimizing the spot size, there has also been huge improvement in the overall intensity throughput of the detector. After finding that a collimated input beam was ideal for the microscope, another concern was presented. The output of the spectrometer itself is not perfectly collimated (it is slightly divergent, at about two degrees), and thus the output of the transfer optics into the microscope was not perfectly collimated. Even if the overall beam divergence was minimized, it was possible that no portion of the IR input beam was truly collimated.

To correct this, I used the internal interferometer aperture in the spectrometer

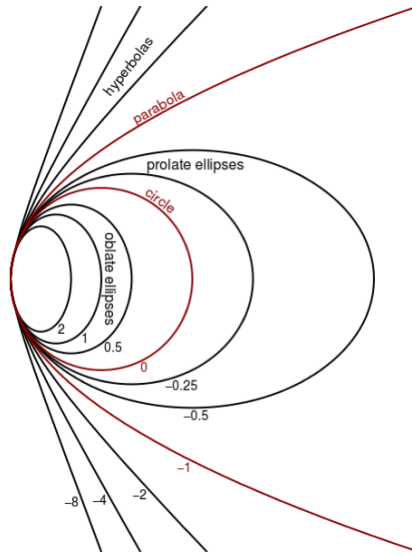


Figure 3.11: Conic Constants of Various Conic Sections

License: 0x30114 at English Wikipedia [CC BY-SA 3.0 (<http://creativecommons.org/licenses/by-sa/3.0>)], via Wikimedia Commons

to isolate the centermost portion of the interferometer output beam, which has the best collimation. Then, I performed an alignment procedure ensuring the collimation of that specific beam section. While this did increase the overall angular spread of diffuse light, the total amount of highly collimated light directed into the microscope increased.

Additionally, after several measurements showed that adjustment of the condenser X-Y (normal to optical axis) position increased throughput, it was discovered that the top aperture and bottom aperture are not perfectly centered on the visual mode eyepiece crosshairs, which was used for aperture alignment. Aligning the apertures to be perfectly overlaying each other decreased clipping on the lower aperture, and increase intensity by several hundred counts. (Note: throughput intensity is measured via the arbitrary intensity units of the output spectrum, which I will refer to throughout this report as "counts").

The largest increase in intensity came as a result of realigning the final detector

position. The detector is adjustable with six degrees of freedom (XYZ translation, pitch, yaw, roll), however the optimal position must be found manual by maximizing the counts. When the final focused beam is optimally incident on the detector element, the resulting counts will be the highest, and the signal-to-noise will be optimized. To optimize counts, initially I had used the final detector ellipsoid mirror to direct the focused beam onto the detector element. However, after a sudden misalignment resulted a recheck of the visual detector spot, it was clear that fine adjustments with this ellipsoid mirror had introduced significant aberrations into the beam focus. Realigning the final mirror to eliminate aberrations, and readjusting the detector position by hand increase the transmission mode counts (with 1.5mm upper aperture) from 7300 to roughly 16,000.

In a later realignment for a different focus position, a slightly different detector position resulted in approximately 23,000 counts. However, this throughput cannot be reached reliably. To improve the alignment procedure, a translation stage should be implemented into the rear of the microscope apparatus so that the position of the detector can be fine-adjusted.

3.3 Spot Size Measurement

Although the theoretical limit of the microscope's spot size is given by the diffraction limited spot, outlined in the theory chapter, the actual spot size of the microscope cannot be trivially measured. There are several reasons for this. First, the beam itself is a Gaussian intensity distribution, with no clear "diameter", so any attempt to measure one directly would be inaccurate and misleading. Additionally, the infrared and visible spot sizes cannot be presumed to be identical, especially as one approaches the diffraction limit (which is dependent upon wavelength).

The proper way to measure the size of the beam at the sample stage focal place

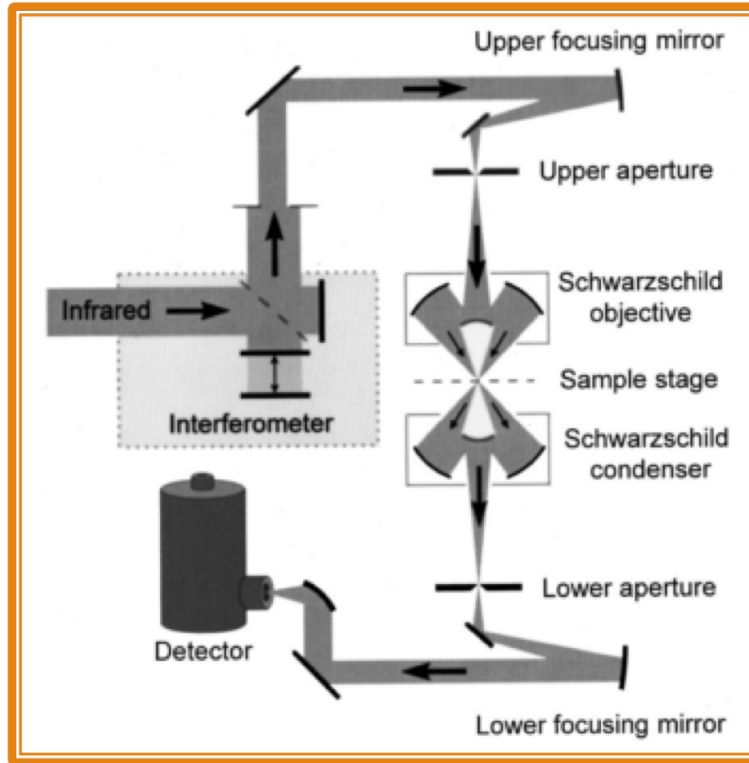


Figure 3.12: Optical Layout of Microscopy Apparatus [1]

(see figure 3.12) is called a "Knife-Edge" measurement, which is commonly used to measure the size of laser beams. The procedure essentially involves the incremental scanning of a sharp blade in front of an incident beam while measuring the beam's intensity with a detector. If the beam has a Gaussian intensity distribution, then the plot of knife edge displacement to measured intensity can be fit with a modified Gauss error function of the form:

$$y = \frac{A}{2} \left(1 + \operatorname{erfc} \left[\frac{\sqrt{2}(x - b)}{c} \right] \right) + C \quad (3.1)$$

where y is the relative intensity and x is the knife edge displacement, presuming the measurements start with the beam completely unobstructed, and end with the knife completely blocking the beam. "erfc" is the actual Gauss error function, and

A, b, c, and C are fitting coefficients. The 'c' fitting coefficient is defined as the "beam waist", which can be interpreted as the diameter (in microns) of a circular cross section of the beam which contains roughly 90% of the total intensity [3]. An example of the code used to complete this analysis is shown in the appendix.

To conduct the knife-edge test, we mounted a knife to an adjustable piezo stage and translated the knife in 15 micron increments. To measure intensity, we simply chose a frequency where no atmospheric vibrational modes are present and recorded the variation in intensity with the displacement. We then fit the data using MATLAB to find the beam waist. An example knife-edge fit is shown in figure 3.13.

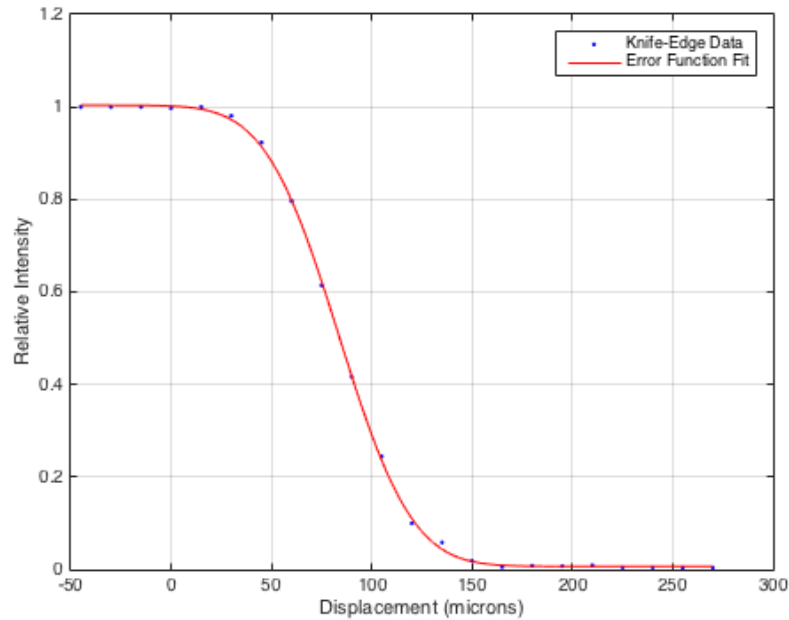


Figure 3.13: Sample Knife-Edge Measurement and Fit

Using this technique, we confirmed that the spot size while a 1.5mm upper aperture is used is roughly 55 microns, and when using a 0.5mm aperture the spot size reduces to 20 microns (measuring at test frequencies around 3000cm^{-1}) At this level, the source intensity at each frequency, has a significant effect on the spot size. Ad-

ditionally, we can repeat the test for multiple different wavelengths and see a general positive trend between wavelength and spot size as we approach the diffraction limit. Below about 1000cm^{-1} , the spot size fluctuates up to around 25-30 microns.

We also used this technique to measure the vertical position of the infrared focus, as opposed to the visual focus. To do this, we visually focused on the knife edge plane and then took data on infrared intensity vs displacement for various vertical positions of the stage, above and below the visual focus. We were able to confirm that the infrared focus is within our margin of error of the visible focus. Therefore, the microscope's visual focus could be used to focus on samples for infrared measurement. Finally, we wanted to confirm that no extreme eccentricity was present in our spot, or that our spot was circular. This was accomplished by repeating the above measurement along both the x and y axes of the sample stage. The plot of spot size versus vertical displacement for both axes is given in figure 3.14.

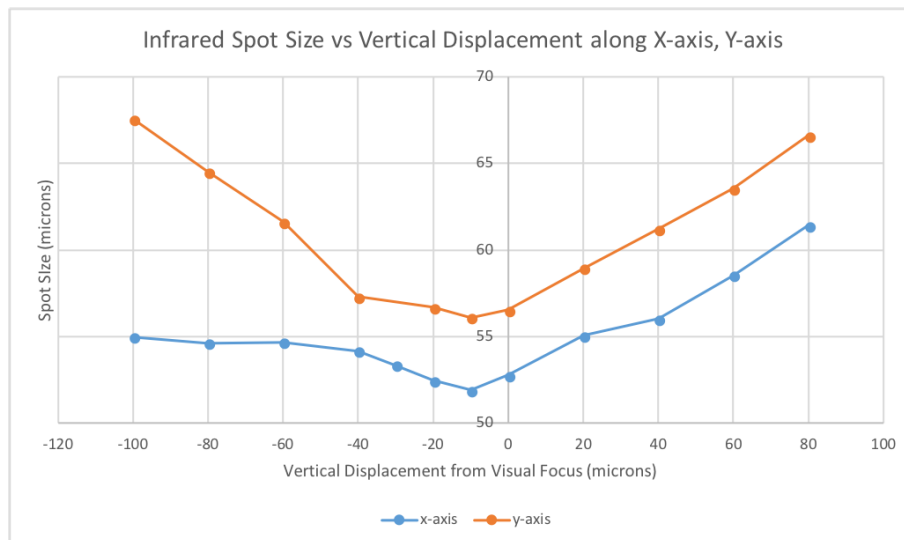


Figure 3.14: Eccentricity and Infrared Focus Measurement

3.4 Electronics

The MCT detector is designed to operate with many different 1980's-era spectrometers manufactured by Nicolet, and therefore has a complex pre-amplifier circuit with many different output channels. To allow compatibility with modern OPUS spectrometry software, we used 3 power supplies to provide 12V +/- rails and a 5V DC supply to the board, and outputted the analog signal from the existing 9-pin cable. Using a custom series of adapters, the signal was eventually ported through a BNC coaxial line to the external accessory port for use with OPUS, from which spectra can be read. An example spectrum, taken with the microscope in IR transmission mode with a MIR source, is shown in figure 3.15.

3.5 Pressure Systems

The Bruker spectrometer is a vacuum spectrometer, which presents an obvious challenge for designing an optical system external to the spectrometer (the microscope). To preserve the spectrometer vacuum, a moving adapter was designed and machined, with a KBr window allowing light to exit from port 3 of the spectrometer while the beam path is in vacuum. KBr was chosen because it is highly transmissive in the MIR, however the port is designed so that other windows could be exchanged if a different spectral region is being examined.

A CAD model of the adapter I constructed is given in figure 3.16. The model has been completely installed, and has been able to withstand rough vacuum pressures below 3.0 milliBar. A similar adapter will be designed for use with the Bolometer detector, to connect the final beam path to the Winston cone with the dry air purge housing planned for the microscope.

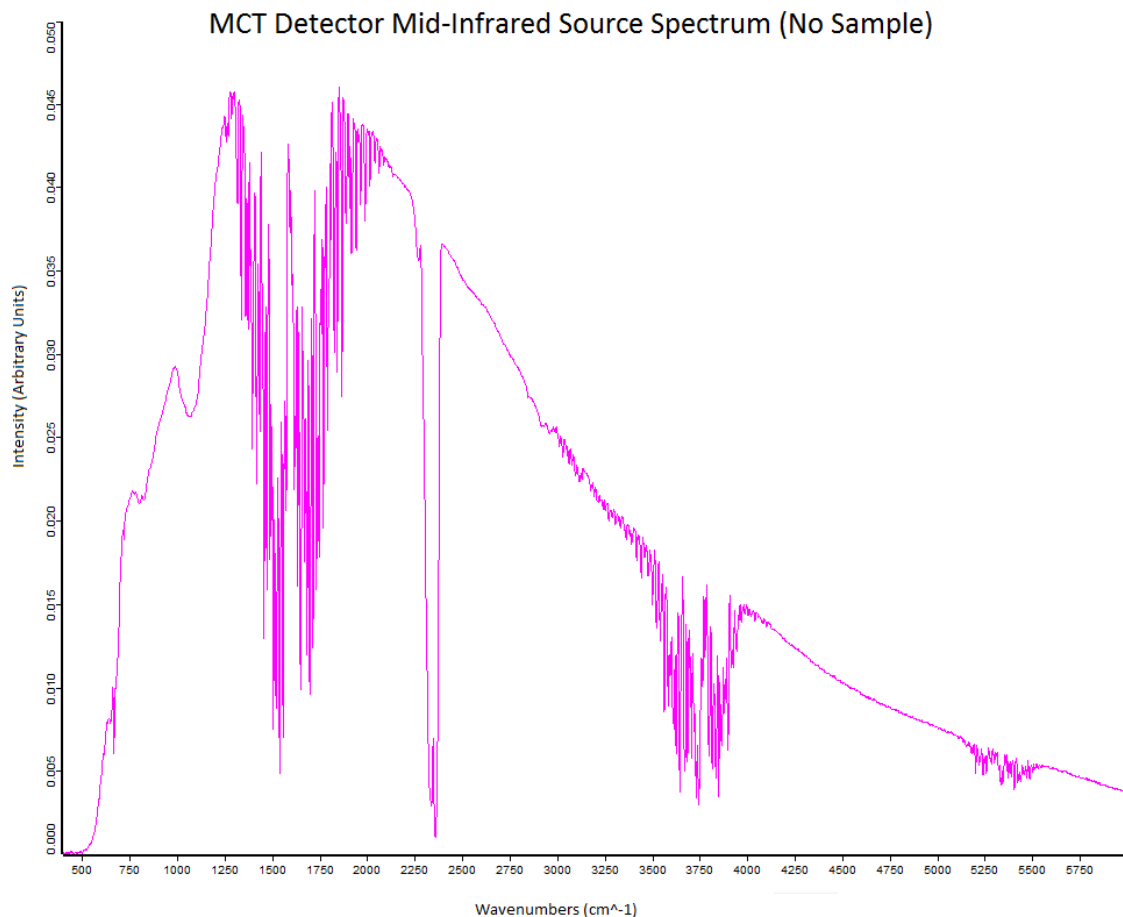


Figure 3.15: Background MIR Spectrum, MCT Detector via Infrared Microscope

3.6 Dry Compressed Air Purge

As discussed in the theory section, the quality of the beampath medium is essential for removing spectral contamination. The beampath from the source through the spectrometer is all in rough vacuum, which eliminates most detectable contamination. However, after the beam exits the spectrometer it is exposed to air. We chose to use compressed air with Parker Baliston purge gas generator. The purge gas generator is essentially a CO₂ scrubber to eliminate carbon dioxide and two desiccant towers to absorb water vapor. Compressed air is pumped from the purge gas generator into a polycarbonate enclosure, framed by aluminum bars and sealed with rubber gaskets.

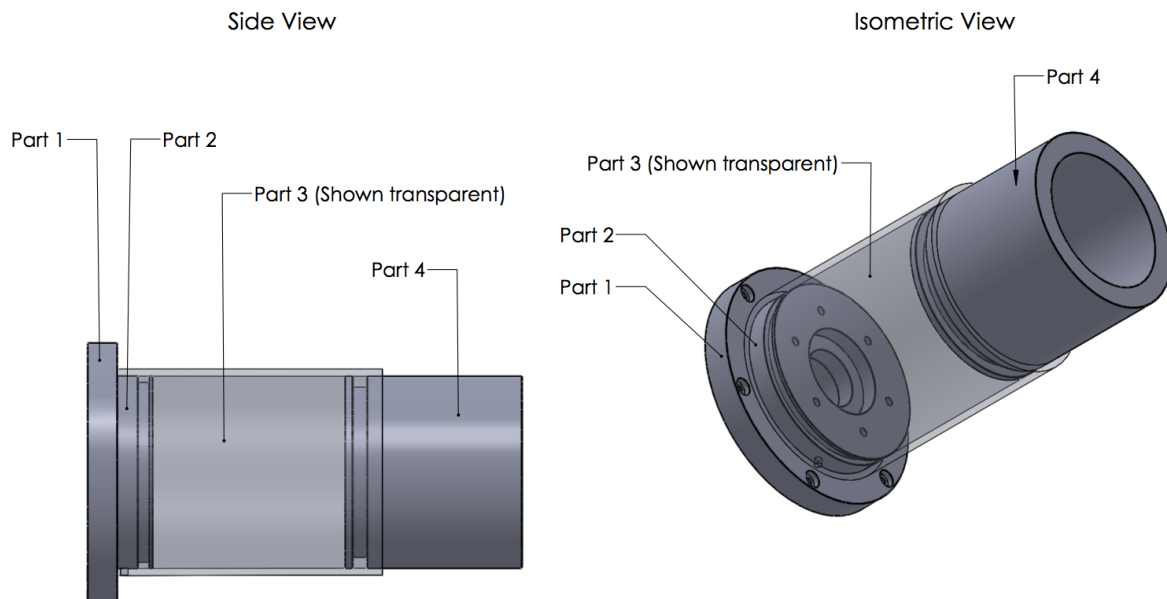


Figure 3.16: Spectrometer-Microscope Vacuum Adapter Model

Part 1 connects the adapter to the existing spectrometer mounting port. Part 2 holds the KBr optical window, allowing the beam to exit. Part 3 is a sliding tube which allows the entire adapter to be retracted for exchange of different vacuum windows, or for the port to be closed when not in use. Part 4 connects the adapter to the dry air purge and the microscope IR input.

Using the purge we are not able to entirely eliminate all evidence of contaminant phonons, however their presence is greatly reduced (see figure 3.17).

Both wide water H_2O features around 1600cm^{-1} and 3750cm^{-1} and the sharp CO_2 feature at 2400cm^{-1} have been mostly eliminated. However, the appearance or disappearance of these features in the background spectra is only a qualitative demonstration of the effectiveness of the purge. To actually examine the impact of the purge gas housing, we need to compare 100% lines with and without the purge gas housing (figure 3.18).

If there are no visible peaks at the locations where we see features in the atmospheric test, then we have successfully decreased the variation of the contaminant

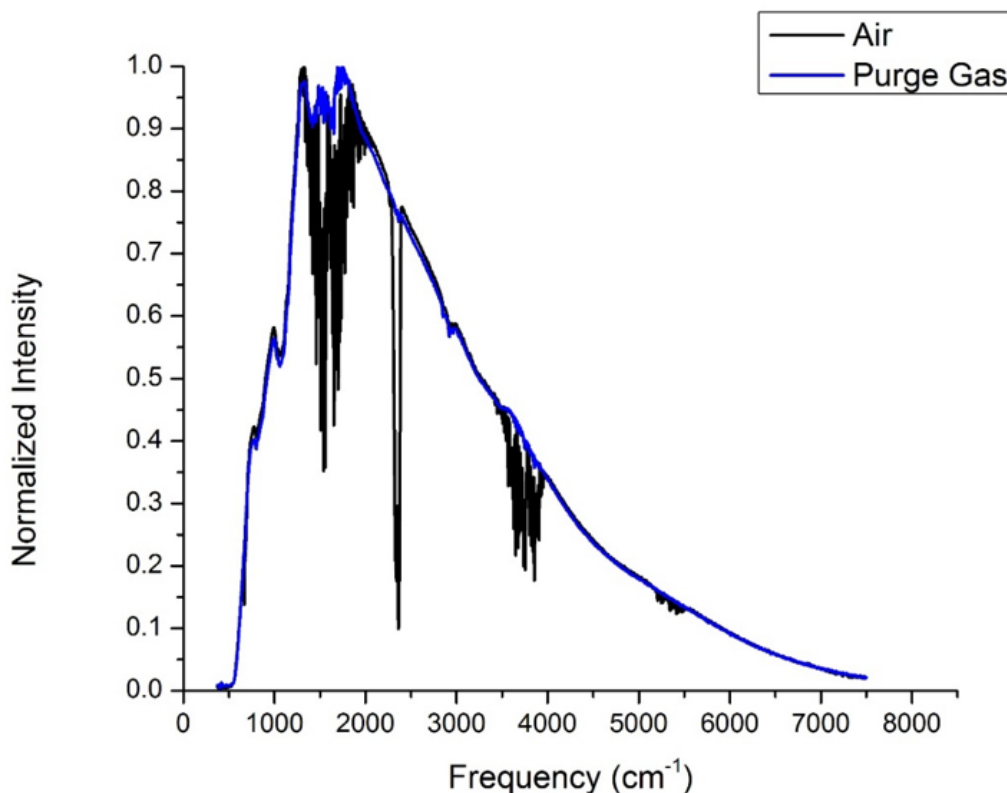


Figure 3.17: MIR Background Spectra, With and Without Purge Housing Installed
phonons to below the detector noise level.

The 100% lines show a clear elimination of the impact of contamination phonons in the beampath, which guarantees that these phonons will not interfere with any actual sample data. The red line indicates the value produced if both the first and second background spectrum for the 100% line were identical, and we can also see that the noise present appears to fluctuate evenly about this line, with no major spectral features present.

Another consideration was how to fill the liquid nitrogen MCT detector dewar without breaking the microscope purge. While the detector coolant allows for many hours of testing, overnight tests would be impossible without breaking the purge. To

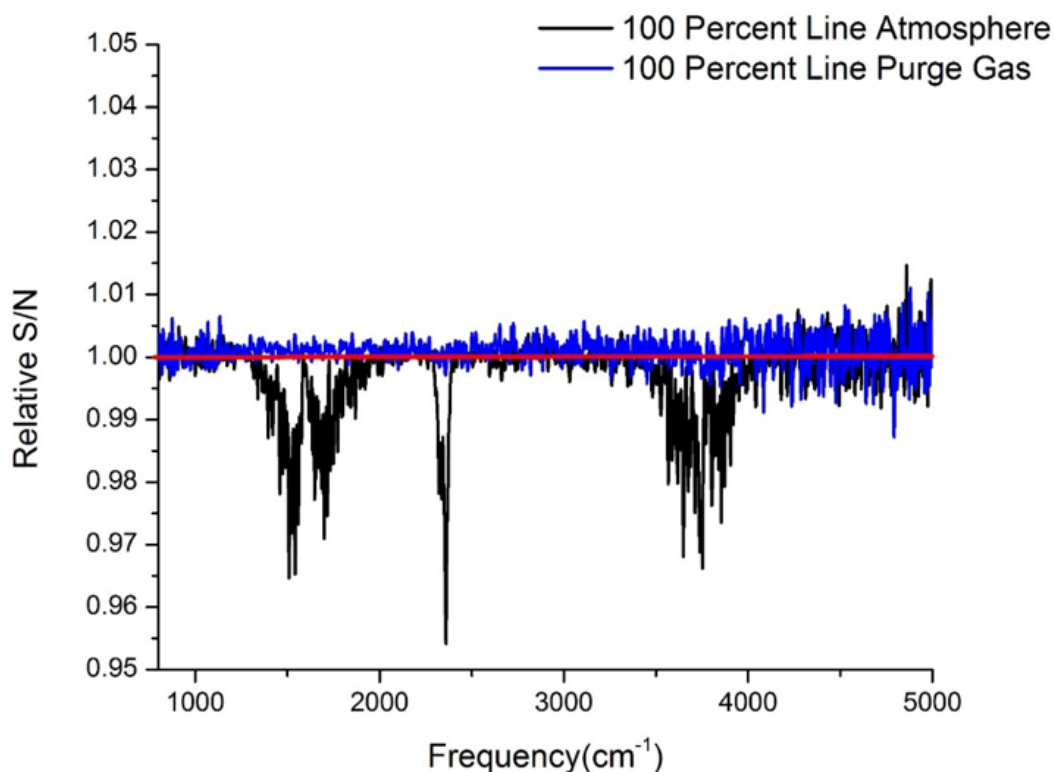


Figure 3.18: MIR 100 Percent Lines, With and Without Purge Housing Installed

allow for refilling of the detector while the system is purged, I designed a nitrogen fill adapter that locks to a bracket secured to the ceiling of the purge housing. From the top of the purge, a funnel can be lower into a tube which connects the top opening of the detector dewar to the outside of the purge. This nitrogen fill can be used to successfully refill the detector without detectably altering the quality of the purge, allowing for potentially continuous measurements over several days if necessary.

3.7 Sample Translation Stage

While the introduction of a purge gas housing has many benefits for the microscope, it also prevents the use of the manual microscope controls while the purge is sealed.

This is most critical with regards to the sample translation stage, which is used to switch between a reference and a sample to obtain a spectrum. To have control over the stage while the microscope is in purge, and to increase the precision of the translation stage, a 1D electronic piezo stage was coupled to the existing manual 2D translation mechanics.

To accomplish this, I designed and constructed a series of parts which integrated the two translation mechanisms, and allowed for samples to be bolt-mounted to prevent sliding or slipping. My design for this new upgraded stage is given in figure 3.19.

After installing the stage, we mounted a test sample of Silicon Nitride to test the operation of the sample stage within the purge. We averaged three transmission spectra taken with a 1.5mm upper aperture, and compared the result to a previously obtained spectrum taken with the existing macroscopic spectroscopy setup. The results are shown in figure 3.20.

This shows that the sample stage is able to repeatably translate between the sample and reference while maintaining the purge. Furthermore, all spectral features identified by the previously obtained silicon nitride measurements are also visible in the microscopy data. The overall difference in intensity is an artifact of the dispersion of silicon nitride, which is a thick sample. In an actual sample measurement, a smaller upper aperture would be used and a substrate would be placed over the reference hole so that the dispersion of the sample and reference would be roughly equivalent.

3.8 Bolometer

As stated previously, the use of a Bolometer detector increases the detectable spectral bandwidth beyond the limits of the MCT detector. The Bolometer detector is liquid Nitrogen and liquid Helium cooled, and has modes for operation at 1.6 and 4.2 degrees

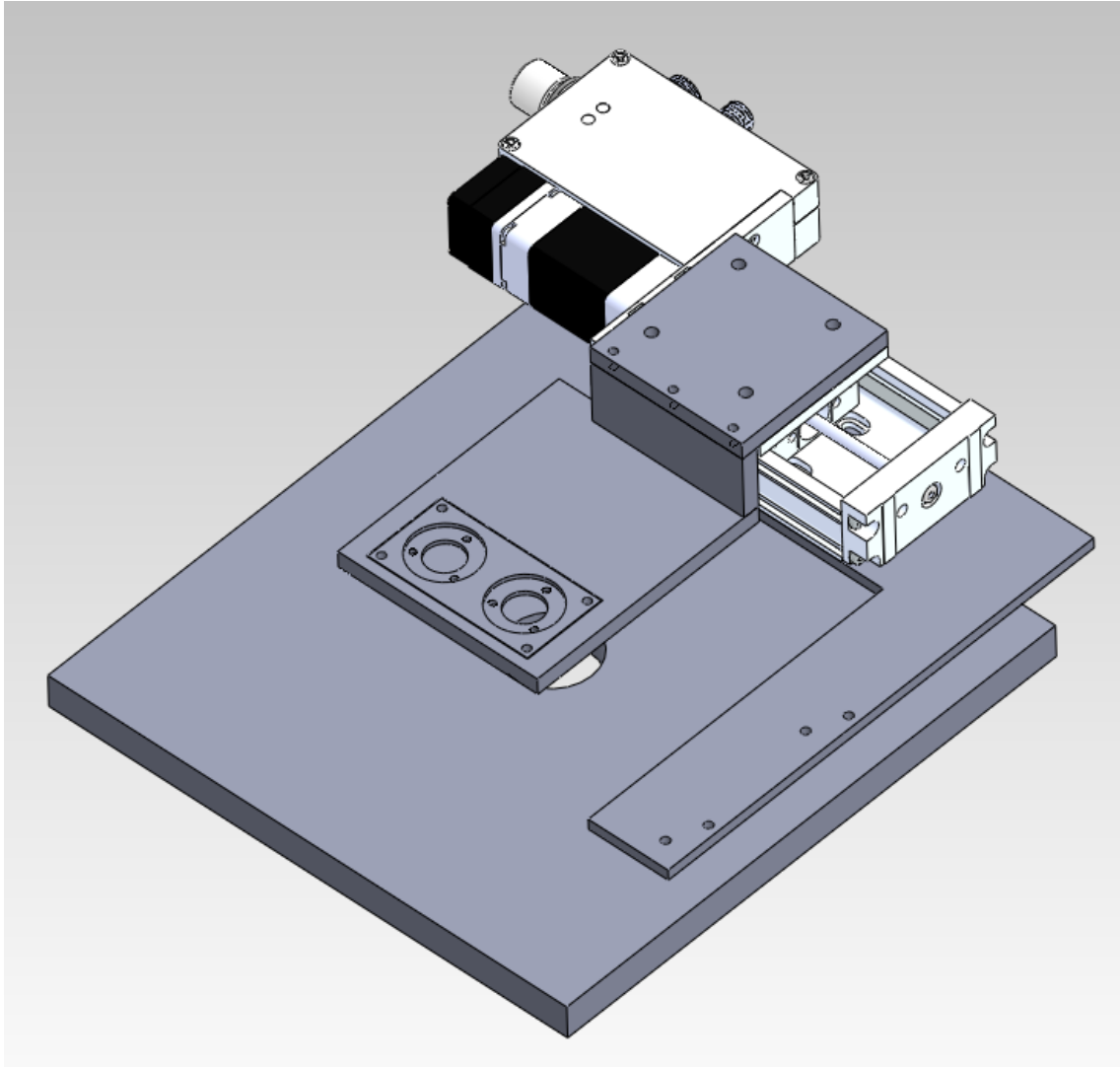


Figure 3.19: 3D CAD of Sample Stage Design

K. Each of these modes uses a different beam input, each of which uses a Winston cone light collector, discussed in the Theory chapter. The Bolometer's spectral range extends to 5cm^{-1} , well into the FIR.

To integrate the Bolometer detector, first the MCT detector baseplate must be exchanged with a baseplate containing the necessary transfer optics. The focused beam of the final detector ellipse will be captured by a custom OAP with a very short focal length, coated in bare gold to maximize reflectance in the FIR. An additional

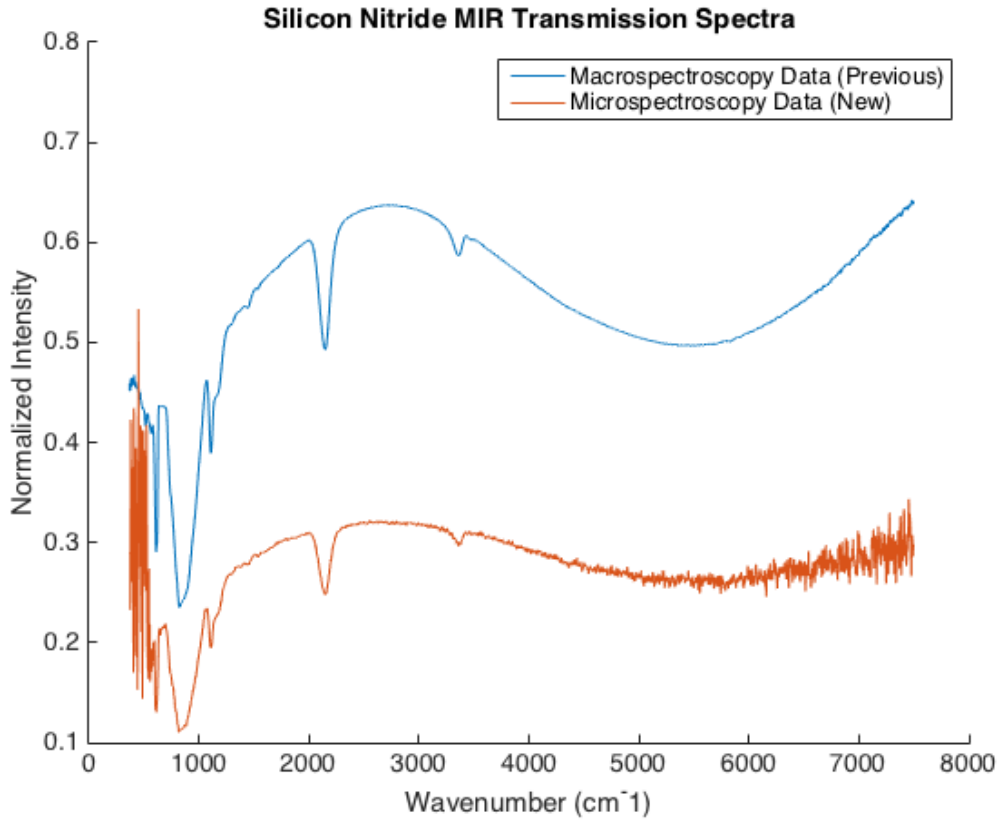


Figure 3.20: Transmission Spectra Obtained with Sample Stage in Purge

plane mirror and a final OAP with a six-inch focal length are used to direct the beam into the Winston cone of the Bolometer. The choice of the final OAP involved a complex analysis of the acceptance angle of the Winston cone, explained in detail in the Appendix. A diagram of the design of the Bolometer transition optics is shown in figures 3.21 and 3.22.

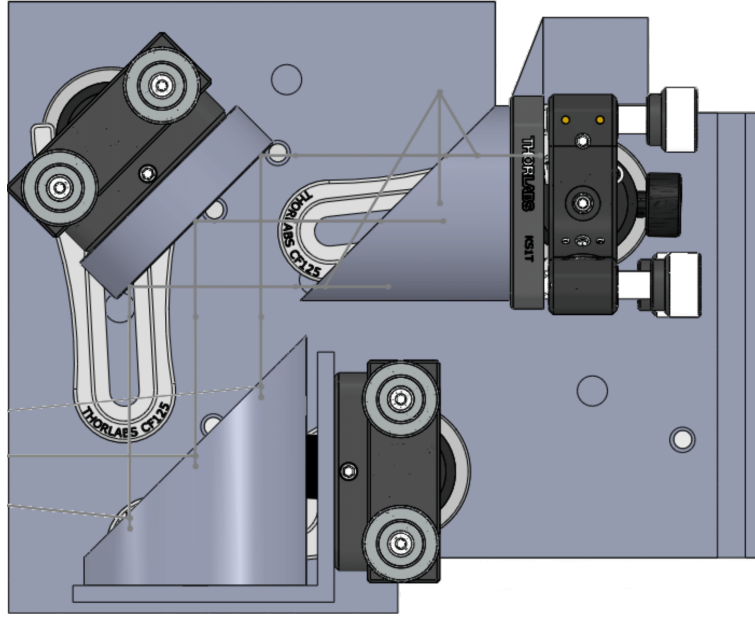


Figure 3.21: Optical Layout of Bolometer Transfer Optics, Mounted on Interchangeable Baseplate

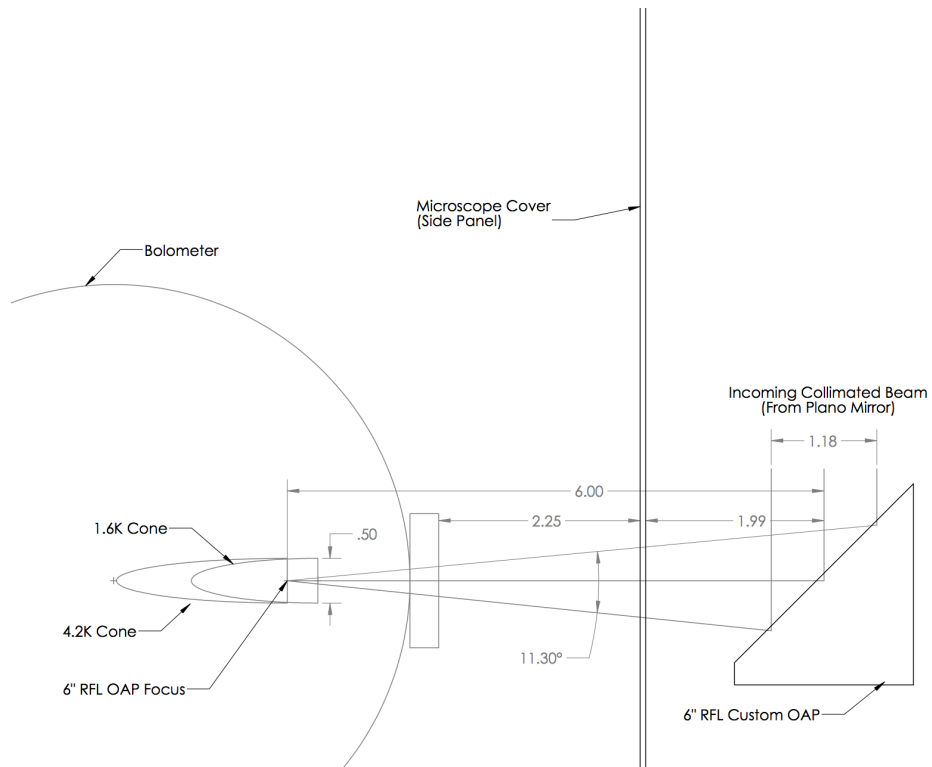


Figure 3.22: Diagram of Final OAP Beam path into Winston Cone

Chapter 4

Results and Conclusions

Presently, the microscope is able to produce 23,000 counts with a 1.5mm upper aperture, corresponding to a 55 micron sample spot size. If using an upper aperture of 0.5mm, the spot size can be reduced below 25 microns, with intensity above 2000 counts. All major atmospheric vibrational resonances can be reliably eliminated, and the stage can be translated between the reference and sample position while maintaining the compressed air purge.

Continued optimization and experimentation could allow further improved intensity and lower spot sizes. For example, the use of a more powerful MIR source could increase the base input intensity by 20-30%. Also, further efforts to optimize the detector position and fix the condenser position will either secure the maximum intensity at 23,000 counts, or continue to improve throughput.

After the verification of previous spectroscopy data with a few test samples, one exciting application of the microscope could be the microscopy analysis of spider silk strands. While bulk (wound strands on a slide) silk samples have been studied via our spectroscopy equipment, no single strand analysis has been possible so far. Brown recluse spider silk strands are on the order of 10 microns, so corresponding spot sizes with reasonable signal to noise would be necessary to take these measurements. In a bulk sample of spider silk, many different orientations of silk are averaged when

a spectroscopy analysis is completed. A single strand measurement could isolate a particular orientation of silk to determine if the different axes of the silk have different optical properties. If so, this could lead to better understanding of why brown recluse spider silk is so strong, and how its strength depends on its tape-like structure. This kind of analysis is a great example of how this apparatus could be used to probe further into ongoing questions in condensed matter.

Appendix A

MATLAB Code Listings

You may wish to include some material in appendices, such as this one.

A.1 Winston Cone

Listing A.1: Winston Cone Minimization Solution

```
h1 = 0.0485; %cone 1 length
h2 = 0.0376; %cone 2 length

D = 0.0127; %cone diameter
a = D/2; %cone radius

%x = theta = phi/2
f = @(x) abs(h1 - a*(cosd(x)+cotd(x))); %cone 1
g = @(x) abs(h2 - a*(cosd(x)+cotd(x))); %cone 2

phi1 = 2*fminsearch(f, 20) %solve for phi, cone 1
phi2 = 2*fminsearch(g, 20) %solve for phi, cone 2

phi1_alt = 2*asind(0.5*3.8^-1) %cone 1, alternative calculation
phi2_alt = 2*asind(0.5*2.44^-1) %cone 2, alternative calculation

bolometer_phi = 2*asind(1.5/(6*2)) %current beam angle into
%bolometer

%sintheta = D/2f

%f = asind(2/(2*4))
```

A.2 Knife Edge Technique

Listing A.2: Knife Edge Data Processing

```
% script gives knife edge fit of Gaussian beam
% script file folder must include "sort_nat.m" and "spotsizes.m"
% data can be in any folder, path must be specified below

%note "horizontal" axis is the axis perpendicular to the detector
...input in the stage plane

% fit "c" coefficient gives beam waist in microns

clear
close all

%% Set Path to Data Files, Set Sampling Frequency

% path should terminate with i.e. '/1.5mm_horizontal/h_0'
% sampling frequency by row of DPT file, not cm-1. View plot to
...find appropriate value (1399 = 4800cm-1)
% increment is height change between data files (i.e. 15)
basePath = ['/Users/ryanwilmington/Desktop/'...
    'Hourglass Measurements/Nov 16th/1.5mm_horizontal/h_'];
samplingfrequency = 1399;
increment = 15;
samples = 7388; % number of frequencies output in DPT file

edges = 18; % number of knife edge data files
height_spacing = 2; % height measurement spacing of knife edge
%measurements

% to suppress plots, paste "set(0,'DefaultFigureVisible','off')"
...into command window
% to restore plots, paste "set(0,'DefaultFigureVisible','on')"

l = 1; %plotting index
x1 = zeros(edges/height_spacing,1);
y1 = x1;

for j = 0:height_spacing:edges
    iter = j;
    endPath = num2str(iter);
    dataPath = strcat(basePath,endPath);

%%
```

```

% go to data path, leave marker of original folder
oldFolder = cd(dataPath);

% obtain data from any files ending in ".dpt"
dataFiles = dir('* .dpt ');
numfiles = length(dataFiles);
mydata = cell(1, numfiles);

cd(oldFolder)

% natural order sort files by name
[tmp, ~]=sort({dataFiles.name});
[tmp, ind] = sort_nat(tmp);
oldFolder = cd(dataPath);
dataFiles = dataFiles(ind);

% extract cell array from struct array
for k = 1:numfiles
    mydata{k} = textread(dataFiles(k).name, '%f ');
end

% parse each data files from full array
% remove frequency data, only include intensity
Data = zeros(samples, numfiles);
D = zeros(samples/2, numfiles);
for i=1:numfiles
    Data(:, i) = mydata{i};
    D(:, i) = Data(2:2:end, i);
end

% isolate data for one frequency
Sample = D(samplingfrequency, :);

% scale intensity values
Y = (Sample./max(Sample)).';

% create horizontal axis
N = increment*(numfiles-1);
X = (0:increment:N).';

cd(oldFolder)

% plot raw data, create fit

%plot(X,Y)

```

```

[beam_waist] = spotsizes(X, Y);

%%
x1(1) = j;
y1(1) = beam_waist;
l = l+1;
end

%%
% plot hourglass result
plot(x1,y1,'b')
set(gca,'FontSize',16)
title('Spot Size vs Z Translation')
xlabel('Displacement (fine adjust clicks)')
ylabel('Spot Size (microns)')

% data output
[x1, y1]

```

Listing A.3: Knife Edge Data Processing (Fitting Function)

```

function [beam_waist] = spotsizes(Displacement, Intensity)
%CREATEFIT(DISPLACEMENT,INTENSITY)
% Create a fit.
%
% Data for 'untitled fit 1' fit:
%   X Input : Displacement Y Output: Intensity
% Output:
%   fitresult : a fit object representing the fit.
%   gof : structure with goodness-of fit info.
%
% See also FIT, CFIT, SFIT.

% Auto-generated by MATLAB on 04-Nov-2017 14:20:20

%% Fit: 'untitled fit 1'.
[xData, yData] = prepareCurveData( Displacement, Intensity );

% Set up fitype and options.
ft = fittype( '(A/2)*(1+erfc((sqrt(2)*(x-b))/c))+C', ...
    'independent', 'x', 'dependent', 'y' );
opts = fitoptions( 'Method', 'NonlinearLeastSquares' );
opts.Display = 'Off';
opts.StartPoint = [0.8407 0.2543 50 20];

% Fit model to data.

```

```

% [fitresult , gof] = fit( xData, yData, ft , opts );

coeff_vector = coeffvalues( fit( xData, yData, ft , opts ));

beam_waist = coeff_vector(4);

%%
Plot fit with data.
figure( 'Name', 'untitled fit 1' );
h = plot( fitresult , xData, yData );
legend( h, 'Intensity vs. Displacement',...
        'untitled fit 1', 'Location', 'NorthEast' );
% Label axes
xlabel Displacement
ylabel Intensity
grid on

```

The above code is adopted from a fitting module produced by Mathworks, included in the MATABL 2015a release. The main modifications include specifying an error function fit with relevant parameters, and adding the beam waist parameter fit as a function output.

Listing A.4: Knife Edge Data Processing (Natural Sort Function)

```

function [cs,index] = sort_nat(c,mode)
%sort_nat: Natural order sort of cell array of strings.
% usage: [S,INDEX] = sort_nat(C)
%
% where,
%   C is a cell array (vector) of strings to be sorted. S is C,
%sorted in natural order. INDEX is the sort order such that
% S = C(INDEX);

% Natural order sorting sorts strings containing digits in a way
% such that the numerical value of the digits is taken into
% account. It is especially useful for sorting file names
% containing index numbers with different numbers of digits.
% Often, people will use leading zeros to get the right sort
% order, but with this function you don't have to do that.
% For example, if C = {'file1.txt','file2.txt','file10.txt'}, a
% normal sort will give you
%
%       {'file1.txt' 'file10.txt' 'file2.txt'}
%

```

```

% whereas, sort_nat will give you
%
%         {'file1.txt' 'file2.txt' 'file10.txt'}
%
% See also: sort

% Version: 1.4, 22 January 2011 Author: Douglas M. Schwarz Email:
% dmschwarz=ieee*org, dmschwarz=urgrad*rochester*edu Real_email =
% regexp(Email,{'=', '*'},{'@', '.'})

% Set default value for mode if necessary.
if nargin < 2
    mode = 'ascend';
end

% Make sure mode is either 'ascend' or 'descend'.
modes = strcmpi(mode,{'ascend', 'descend'});
is_descend = modes(2);
if ~any(modes)
    error('sort_nat:sortDirection',...
        'sorting direction must be ''ascend'' or ''descend''.')
end

% Replace runs of digits with '0'.
c2 = regexp(c, '\d+', '0');

% Compute char version of c2 and locations of zeros.
s1 = char(c2);
z = s1 == '0';

% Extract the runs of digits and their start and end indices.
[digruns, first, last] = regexp(c, '\d+', 'match', 'start', 'end');

% Create matrix of numerical values of runs of digits and a
% matrix of the number of digits in each run.
num_str = length(c);
max_len = size(s1, 2);
num_val = NaN(num_str, max_len);
num_dig = NaN(num_str, max_len);
for i = 1:num_str
    num_val(i, z(i, :)) = sscanf(sprintf('%s ', digruns{i}{:}), '%f');
    num_dig(i, z(i, :)) = last{i} - first{i} + 1;
end

```

```

% Find columns that have at least one non-NaN. Make sure
% activecols is a 1-by-n vector even if n = 0.
activecols = reshape(find(~all(isnan(num_val))),1,[]);
n = length(activecols);

% Compute which columns in the composite matrix get the numbers.
numcols = activecols + (1:2:2*n);

% Compute which columns in the composite matrix get the number
% of digits.
ndigcols = numcols + 1;

% Compute which columns in the composite matrix get chars.
charcols = true(1,max_len + 2*n);
charcols(numcols) = false;
charcols(ndigcols) = false;

% Create and fill composite matrix, comp.
comp = zeros(num_str,max_len + 2*n);
comp(:,charcols) = double(s1);
comp(:,numcols) = num_val(:,activecols);
comp(:,ndigcols) = num_dig(:,activecols);

% Sort rows of composite matrix and use index to sort c in
% ascending or descending order, depending on mode.
[unused,index] = sortrows(comp);
if is_descend
    index = index(end:-1:1);
end
index = reshape(index,size(c));
cs = c(index);

```

The above code is a natural order sort algorithm written by Douglas M. Schwarz under the following license:

Copyright (c) 2008, Douglas M. Schwarz All rights reserved.

Appendix B

Winston Cone

The inputs to the Bolometer are two Winston cones, one for a 4.2K detector element and another for a 1.6K detector element. Winston cones can collect light at a variety of input angles and direct it toward a common target. The calculation for the acceptance angle of a Winston cone is based on the patent for the Compound Parabolic Concentrator (CPC) [7][5].

B.1 Acceptance Angle

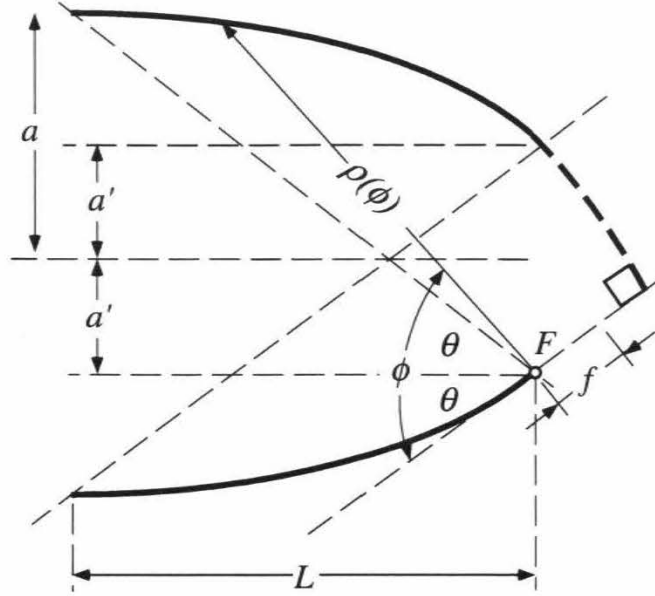


Figure B.1: Winston Cone Diagram

The following relationships are given by the patent for the CPC, as detailed by Weisstein's 1996 Thesis [4] and verified in Winston's 1980 paper published in Applied Optics [6]. The meanings of all variables and constants are given by the diagram above, except for L , which is the total length of the Winston cone.

$$F = a'(1 + \sin\theta) \quad (\text{B.1})$$

$$L = \frac{F \cos\theta}{\sin^2\theta} \quad (\text{B.2})$$

$$2a' = 2a \sin\theta \quad (\text{B.3})$$

To find the incoming angle θ , we can substitute equation 3 into equation 1, and then equation 1 into equation 2 as follows:

$$2a' = 2a \sin\theta$$

$$a' = a \sin\theta$$

$$F = a'(1 + \sin\theta)$$

$$F = (a\sin\theta)(1 + \sin\theta)$$

$$L = \frac{F\cos\theta}{\sin^2\theta}$$

$$L = \frac{(a\sin\theta)(1 + \sin\theta)\cos\theta}{\sin^2\theta}$$

$$L = \frac{a\cos\theta(1 + \sin\theta)}{\sin\theta}$$

$$L = \frac{a\cos\theta}{\sin\theta} + \frac{a\cos\theta\sin\theta}{\sin\theta}$$

$$L = a\cot\theta + a\cos\theta$$

$$L = a(\cot\theta + \cos\theta)$$

Note that θ , or the incoming beam angle, is defined as one half of the acceptance angle ϕ . The stated formulas can be solved for the incoming angle θ , where the acceptance angle ϕ is defined as 2θ .

Now we have an expression which relates the height of the Winston cone L and the size of the initial aperture a , which are both known. However, to solve this equation for the acceptance angle ϕ , it is helpful to use computational software. The solutions below were calculated using a MATLAB minimization script, included in the appendix as listing A.1.

There are four general solutions to this equation, all of which are too lengthy to be included here. However, for any real, positive values for L and a , there are two real solutions (one positive, one negative) and two imaginary solutions. Negative and imaginary solutions are thrown out.

The acceptance angle for a Winston cone with our specifications is given below.

$$L = 48.5mm = 0.0485m$$

$$a = 6.4mm = 0.0064m$$

$$\phi = 17.1 \text{ degrees}$$

For our second cone:

$$L = 37.6mm = 0.0376m$$

$$a = 6.4mm = 0.0064m$$

$$\phi = 22.9 \text{ degrees}$$

B.2 Alternative Calculation

Alternatively, the acceptance angle of any optical system can be modeled by an f-number (N), where,

$$N = f/D$$

f being the focus of the optic and D being the diameter of the beam at it's source or termination.¹

The acceptance angle of a system can be related to its f-number through the relationship,

$$\sin\theta = \frac{D}{2f} \quad (\text{B.4})$$

Substituting the f-number for D and f , then acceptance angle of the optic can be calculated. Using this method, our Winston cones are defined as follows:

For cone 1:

$$N = 3.8$$

$$\phi = 15.1 \text{ degrees}$$

For cone 2:

$$N = 2.44$$

$$\phi = 23.6 \text{ degrees}$$

These two methodologies provide acceptably similar values for the acceptance angle of each Winston cone.

B.3 Parabolic Mirror Selection

Assuming that the method above is accurate for the calculation of the incoming beam angle resultant from a parabolic mirror, here are the angles for a one-inch, two-inch, three-inch and four-inch parabolic, assuming a one-inch mirror.

$$f = 1''$$

$$\phi = 53.1 \text{ degrees}$$

$$f = 3''$$

$$\phi = 18.9 \text{ degrees}$$

$$f = 2''$$

$$\phi = 28.1 \text{ degrees}$$

$$f = 4''$$

$$\phi = 14.3 \text{ degrees}$$

For a two-inch mirror, here are the corresponding angles:

$$f = 1''$$

$$\phi = 90.0 \text{ degrees}$$

$$f = 2''$$

$$\phi = 53.1 \text{ degrees}$$

$$f = 3''$$

$$\phi = 36.9 \text{ degrees}$$

$$f = 4''$$

$$\phi = 28.1 \text{ degrees}$$

Note: The current parabolic mirror directed into the Bolometer is a 1.5-inch mirror with a six-inch focal length, which gives an acceptance angle $\phi = 14.4 \text{ degrees}$. This is within the acceptance angle of both bolometer cones.

Bibliography

- [1] G. L. Carr, "Resolution limits for infrared microspectroscopy explored with synchrotron radiation," *Rev. Sci. Instrum.* 72, 1613-1619 (2001).
- [2] H. J. Humecki, *Practical Guide to Infrared Microspectroscopy* (Marcel Dekker, 1995).
- [3] Y. Suzaki and A. Tachibana, "Measurement of the μm sized radius of Gaussian laser beam using the scanning knife-edge," *Appl. Opt.* 14, 2809-2810 (1975).
- [4] E.W. Weisstein, *Millimeter/Submillimeter Fourier Transform Spectroscopy of Jovian Planet Atmospheres*, thesis, California Institute of Technology, 2013.
- [5] W. T. Welford and R. Winston, *The Optics of Non-Imaging Concentrators: Light and Solar Energy* (Academic Press, New York, 1978).
- [6] R. Winston and W.T. Welford, *Applied Optics* 19, 347 (1980).
- [7] Winston, Roland. *Compound Parabolic Concentrator with Cavity for Tubular Absorbers*. US Patent US 4387961 A, filed January 30, 1981, and issued June 14, 1983.

Additional Sources:

Hildebrand, R. H. and R. Winston 1982. Throughput of diffraction-limited field optics system for infrared and millimetric telescopes. *Appl. Opt.* 21. 1844-1846.

Hildebrand, R. H. 1985. Erratum to: Throughput of diffraction-limited field optics system for infrared and millimetric telescopes. *Appl. Opt.* 24. 616.

Winston, R. 1970. Light collection within the framework of geometric optics. *J. Opt. Soc. Amer.* 60, 245-247.